

511/6011-2577

WINDBREAK EFFECTIVENESS FOR STORAGE-PILE FUGITIVE-DUST CONTROL  
A Wind Tunnel Study

by

Barbara J. Billman

and

S.P.S. Arya

Department of Marine, Earth and Atmospheric Sciences  
North Carolina State University  
Raleigh, NC 27695-8208

Cooperative Agreement Number CR-811973

Project Officer

William H. Snyder  
Meteorology and Assessment Division  
Atmospheric Sciences Research Laboratory  
Research Triangle Park, North Carolina 27711

ATMOSPHERIC SCIENCES RESEARCH LABORATORY  
OFFICE OF RESEARCH AND DEVELOPMENT  
U.S. ENVIRONMENTAL PROTECTION AGENCY  
RESEARCH TRIANGLE PARK, NORTH CAROLINA 27711

## DISCLAIMER

This report has been reviewed by the Atmospheric Sciences Research Laboratory, U.S. Environmental Protection Agency, and approved for publication. Approval does not signify that the contents necessarily reflect the views and policies of the U.S. Environmental Protection Agency, nor does mention of trade names or commercial products constitute endorsement or recommendation for use.

## ABSTRACT

Results of wind-tunnel experiments to determine the optimal size and location of porous windbreaks for controlling fugitive-dust emissions from storage piles in a simulated neutral atmospheric boundary layer are presented. Straight sections of windbreak material were placed upwind of two non-erodible, typically shaped piles and were also placed on the top of one of the piles. Wind speed, measured near the pile surface at various locations with heated thermistors, was isolated here as the primary factor affecting particle uptake. Wind speed distributions about the piles in the absence of any windbreak and the flow structure downwind of a three-dimensional porous windbreak are presented. Relative wind speed reduction factors are described and efficiencies based on the relationship between wind speed and particle uptake are given. The largest and most solid windbreak caused the greatest wind speed reduction, but similar wind speed reductions were obtained from several smaller windbreaks. A 50% porous windbreak of height equal to the pile height and length equal to the pile length at the base, located one pile height from the base of both piles was found to be quite effective in reducing wind speeds over much of the pile. Windbreaks placed on the top of a flat-topped pile caused large wind speed reductions on the pile top, but small, if any, reductions on the windward pile face. Windbreak effectiveness decreased as the angle between the windbreak and the wind direction decreased.

## CONTENTS

DISCLAIMER .....	ii
ABSTRACT .....	iii
FIGURES .....	v
TABLES .....	viii
SYMBOLS .....	ix
ACKNOWLEDGEMENTS .....	xii
1. INTRODUCTION .....	1
2. LITERATURE REVIEW .....	4
2.1 Fugitive-Dust Emission Rates .....	4
2.2 Flow About Windbreaks .....	7
2.3 Windbreaks for Storage-Pile Fugitive-Dust Control .....	10
3. EXPERIMENTAL DESIGN AND INSTRUMENTATION .....	13
3.1 Experimental Design .....	13
3.2 Instrumentation .....	22
4. FLOW ABOUT A POROUS WINDBREAK .....	41
5. FLOW ABOUT STORAGE PILES .....	51
5.1 Conical Pile .....	51
5.2 Oval, Flat-topped Pile .....	53
6. WINDBREAK EFFECTS ON FLOW ABOUT STORAGE PILES .....	58
6.1 Windbreaks Upstream of the Pile .....	58
6.1.1 Relation to flow structure .....	58
6.1.2 Results.....	59
6.2 Windbreaks on the Pile Top .....	75
7. FURTHER ANALYSES AND DISCUSSION OF RESULTS .....	80
7.1 Relation to Particle Uptake .....	80
7.2 Comparison to Previous Studies .....	88
8. CONCLUSIONS .....	90
9. REFERENCES .....	93

## FIGURES

<u>Number</u>	<u>Page</u>
2.1 Sketches of streamlines about windbreaks: (a) solid, (b) porous.....	8
3.1 Boundary-layer velocity profile: (a) linear, (b) semi-logarithmic.....	14
3.2 Sketch of oval, flat-topped pile.....	16
3.3 Geometry of conical pile and windbreak.....	20
3.4 Example hot-wire anemometer calibration plots.....	25
3.5 Sketch of a pulsed-wire anemometer probe.....	27
3.6 Typical signals observed from various stages of the pulsed-wire anemometer.....	29
3.7 Example pulsed-wire anemometer calibration plot.....	31
3.8 Resistance-temperature thermistor curves.....	33
3.9 Thermistor circuit.....	34
3.10 Dissipation factor vs. wind speed for Fenwal GB31J1 thermistors.....	34
3.11 Top view of conical pile. Stars: Thermistor positions on pile. Dots: Effective thermistor positions due to pile rotation.....	37
3.12 Top view of oval, flat-topped pile. Dots: Thermistor positions.	37
3.13 Comparison of thermistor and single-wire wind speed measurements.....	38
4.1 "Streamlines" and normalized velocity vectors downstream of a porous windbreak.....	42
4.2 Relative wind speed deficit downstream of a porous windbreak...	44
4.3 Turbulence intensity downstream of a porous windbreak.....	46
4.4 Normalized r.m.s. longitudinal velocity fluctuation downstream of a porous windbreak.....	47
4.5 Profiles of normalized wind speed downstream of a porous windbreak.....	48

<u>Number</u>	<u>Page</u>
4.6 Profiles of normalized longitudinal velocity fluctuation downstream of a porous windbreak.....	50
5.1 $u/u_r$ about conical pile for no windbreak case.....	52
5.2 $u/u_r$ about oval, flat-topped pile for no windbreak case.....	54
5.3 Corrected $u/u_r$ about oval, flat-topped pile for no windbreak case.....	55
5.4 Corrected $u/u_r$ about oval, flat-topped pile at an angle to incident flow for no windbreak case: (a) $20^\circ$ , (b) $40^\circ$ .....	57
6.1 Superposition of conical pile positions and undisturbed "streamlines" downstream of a porous windbreak of height: (a) $0.5H$ , (b) $1.0H$ , (c) $1.5H$ .....	60
6.2 Superposition of oval, flat-topped pile positions and undisturbed "streamlines" downstream of a porous windbreak height: (a) $0.5H$ , (b) $1.0H$ , (c) $1.5H$ .....	61
6.3 Wind speed reduction factor for the 65% porous windbreak of height $0.5H$ and length $1.0D$ placed $1H$ from the conical pile base.....	63
6.4 Wind speed reduction factor for the 65% porous windbreak of height $0.5H$ and length $1.0B$ placed $1H$ from the oval, flat-topped pile base.....	63
6.5 Wind speed reduction factor for the 50% porous windbreak of height $1.5H$ placed $1H$ from the oval, flat-topped pile base with length $0.6B$ (solid line) and $1.0B$ (dashed line).....	67
6.6 Wind speed reduction factor for the windbreak of height $1.0H$ and length $1.0D$ placed $1H$ from the conical pile base with porosity 65% (solid line) and 50% (dashed line).....	69
6.7 Wind speed reduction factor for the windbreak of height $1.0H$ and length $0.6B$ placed $1H$ from the oval, flat-topped pile base with porosity 65% (solid line) and 50% (dashed line).....	69
6.8 Wind speed reduction factor for the 50% porous windbreak of height $1.5H$ and length $1.5D$ placed $1H$ (solid line) and $3H$ (dashed line) from the conical pile base.....	71
6.9 Wind speed reduction factor for the 50% porous windbreak of height $1.5H$ and length $0.6B$ placed $1H$ (solid line) and $3H$ (dashed line) from the oval, flat-topped pile base.....	71

<u>Number</u>	<u>Page</u>
6.10 Wind speed reduction factor for the 50% porous windbreak of height $1.0H$ and length $1.0D$ placed $1H$ from the conical pile base oriented (a) normal, (b) $20^\circ$ , and (c) $40^\circ$ to the flow direction.....	74
6.11 Sketch of windbreak positions with respect to thermistor positions on the top of the oval, flat-topped pile.....	76
6.12 Wind speed reduction factor for the 65% porous windbreak placed near the pile leading edge: (a) height $0.27H$ and length $0.5T$ , (b) height $0.14H$ and length $0.5T$ , (c) height $0.27H$ and length $0.16T$ .....	77
6.13 Wind speed reduction factor for the 65% porous windbreak of height $0.27H$ and length $0.5T$ placed near the pile centerline. Pile is: (a) normal, (b) $40^\circ$ to the incident flow.....	78
7.1 Efficiency ( $E_3$ ) vs. height for windbreaks placed $3H$ from the pile base: (a) conical pile, (b) oval, flat-topped pile.....	86

## TABLES

<u>Number</u>	<u>Page</u>
3.1 Combinations of windbreak parameters used with the conical pile.....	21
3.2 Combinations of windbreak parameters used with the oval, flat-topped pile.....	23
6.1 $u_{\max}/u_r$ for the various windbreaks placed upstream of the conical pile.....	72
6.2 $u_{\max}/u_r$ for the various windbreaks placed upstream of the oval, flat-topped pile.....	72
7.1 Efficiency ( $E_1$ ) for the various windbreaks placed upstream of the conical pile.....	83
7.2 Efficiency ( $E_1$ ) for the various windbreaks placed upstream of the oval, flat-topped pile.....	83
7.3 Efficiency ( $E_3$ ) for the various windbreaks placed upstream of the conical pile.....	85
7.4 Efficiency ( $E_3$ ) for the various windbreaks placed upstream of the oval, flat-topped pile.....	85

## SYMBOLS

a	constant
A	surface area [ $L^2$ ]
b	constant
B	oval, flat-topped pile base length [ $L$ ]
c	constant
$c_p$	pressure drop coefficient
C	constant
d	distance between pulsed wire and sensor wire [ $L$ ]
D	conical pile base diameter [ $L$ ]
E	voltage [volt] or windbreak efficiency or effectiveness factor
EF	emission factor [ $M/L^2T$ ]
f	percentage of time that unobstructed wind speed exceeds 5.4 m/s at mean pile height
F	constant
h	windbreak height
H	pile height
i	electric current [amp]
k	von Karman's constant
K	thermistor dissipation factor [ $ML^2/T^3\theta$ ]
L	windbreak length or a characteristic length [ $L$ ]
n	exponent 1 or 3
p	number of days with $> 0.25$ mm precipitation per year
P	static pressure [ $M/LT^2$ ] or distance between windbreak and pile upstream base [ $L$ ]
PE	Thorntwaite's precipitation-evaporation index
Q	storage-pile erosion rate [ $M/T$ ]

R	resistance [ohm] or wind speed reduction factor
s	pile surface area [ $L^2$ ]
S	silt content
t	time or time-of-flight [T]
T	oval, flat-topped pile top length [L] or temperature [ $\theta$ ]
u	wind speed [L/T]
u'	longitudinal component of velocity fluctuation [L/T]
u <sub>*</sub>	friction velocity [L/T]
U	mean wind speed or a characteristic wind speed [L/T]
V	voltage [volt]
w	oval, flat-topped pile base width [L]
w'	vertical component of velocity fluctuation [L/T]
x	Cartesian coordinate (streamwise) [L]
y	Cartesian coordinate (lateral) [L]
z	Cartesian coordinate (vertical) [L]
z <sub>0</sub>	surface roughness length [L]
$\alpha$	exponent in King's law
$\beta$	thermistor constant [ $\theta$ ]
$\gamma$	angle between direction normal to the pulsed-wire plane and the instantaneous velocity vector
$\delta$	boundary-layer height [L]
$\rho$	air density [M/L <sup>3</sup> ]
$\rho_b$	bulk density [M/L <sup>3</sup> ]

#### Subscripts and special symbols

- ( )<sub>0</sub> no windbreak case or free-stream value
- ( )<sub>1</sub> value based on linear relation between wind speed and particle uptake

- ( )<sub>3</sub> value based on cubic relation between wind speed and particle uptake
- ( )<sub>a</sub> ambient value
- ( )<sub>i</sub> specific pile location value or index
- ( )<sub>max</sub> maximum value
- ( )<sub>r</sub> reference value
- ( )<sub>R</sub> reference value
- ( )<sub>t</sub> threshold value
- ( )<sub>T</sub> thermistor value
- $\overline{(\quad)}$  area-averaged value

## ACKNOWLEDGEMENTS

The authors wish to acknowledge the advice and help given by Dr. W.H. Snyder and his staff at the EPA Fluid Modeling Facility. The cooperation and help from Messrs. W.B. Kuykendal and D.L. Harmon (EPA-AEERL) is appreciated. Mr. W.R. Pendergrass (Oak Ridge Associated Universities) provided the pulsed-wire anemometer. Mr. R. Lawrence (KPN, International) provided the commercial windbreak material.

## 1. INTRODUCTION

Total suspended particulate (TSP) levels in many regions of the country do not meet the National Ambient Air Quality Standard; fugitive dust from sources such as storage piles, materials transfer points, unpaved roads, and agricultural tilling contribute significantly to TSP levels in some regions. Wind erosion causes an estimated 30% of storage-pile fugitive-dust emissions; load-in and load-out processes (30%) and vehicular traffic (40%) cause the remainder (Cowherd et al., 1974).

Many states regulate fugitive-dust emissions by forbidding visible fugitive dust beyond the property line surrounding the source; some states have more strict storage-pile fugitive-dust regulations (e.g. Bureau of National Affairs, 1982 and 1983). Although limiting emissions from a fugitive dust source may not be required, a given industrial facility may use the Environmental Protection Agency (EPA) "bubble" policy to their benefit by controlling fugitive dust rather than the more costly process of upgrading the particulate controls on their stacks to make them more efficient.

Radioactive particulate is also regulated. EPA's "Environmental Radiation Protection Standards for Nuclear Power Operations" (40 CFR 190) provides limits for radiation doses received by the public. The Nuclear Regulatory Commission (NRC) amended 10 CFR 20, requiring that NRC licensees comply with the EPA regulations. Criterion 8 of that amendment states that to control dusting from tailings, dry tailings shall be wetted or chemically stabilized, unless the "tailings are effectively sheltered from the wind, such as may be the case where they

are disposed of below grade and the tailings surface is not exposed to wind. . ."

Storage piles, in addition to tailings, are found at mines, mineral processing plants, coal-fired electric generating plants, within the iron and steel industry, etc. and contain coal, coke, limestone, aggregate, sand, etc.

Early air pollution control efforts emphasized controlling emissions from stacks rather than fugitive emission sources because the greater bulk of pollutants came from stacks. Now that efficient control methods for particulate matter from stacks are available, control methods for fugitive dust sources are being tested. The EPA Air & Energy Engineering Research Laboratory (formerly Industrial Environmental Research Laboratory) requested that the EPA Atmospheric Sciences Research Laboratory (formerly Environmental Sciences Research Laboratory) conduct a wind tunnel study to assess windbreak effectiveness for the control of fugitive dust from storage piles. This study was undertaken as part of a cooperative agreement between the EPA and North Carolina State University.

Since wind direction is variable, encircling a storage-pile with a windbreak will shield it from winds in all directions. However, this may not be practical, particularly for an active pile, or economically feasible due to size. A straight windbreak placed to protect a pile from the prevailing winds may be more practical. A windbreak may also be placed on top of some piles to protect certain areas, say where material is removed from or added to the pile. In the present study, wind speed is isolated as the primary factor affecting particle uptake,

although moisture content, particle size, and bulk density affect fugitive-dust emissions as well. Wind speed was measured near the pile surface with and without windbreaks of several sizes and porosities located various distances upwind or on the top of two typically shaped storage piles. No effort was made to simulate fugitive dust emissions. Effect of wind direction was also observed. The wind speed patterns were analyzed to determine the optimal windbreak porosity, height, length, and location and to develop windbreak design guidelines for storage-pile fugitive-dust control.

The following sections consist of a literature review, a description of the experimental design, instrumentation, and the flows about a representative windbreak and about the two storage piles. Wind speed patterns for various windbreak cases are presented and effects of the windbreak parameters are noted. Finally, the wind speed distributions are related to particle uptake.

## 2. LITERATURE REVIEW

Reviews of three topics are presented as background material to the present study. The relationship between wind speed and fugitive-dust emission rate is examined first. Second, the structure of the flow about a windbreak placed on a horizontal surface is examined. Finally, a review of the literature dealing with windbreaks for storage-pile fugitive-dust control is presented.

### 2.1 FUGITIVE-DUST EMISSION RATES

Mechanical forces by such implements as bulldozers acting on the pile surface and by falling material impacting the surface, freezing and thawing, etc., create particles that may become airborne. Storage-pile fugitive-dust emission rates depend upon the stored material's bulk density, moisture content and particle size distribution, the storage pile geometry, the wind velocity near the pile surface and other parameters. However, particle uptake does not occur unless the wind speed is greater than a given value, the threshold velocity, which is dependent upon the type of stored material, its moisture content and particle size distribution.

Several relationships between wind speed and particle uptake rate are found in the literature. Bagnold (1941) suggested that the particle uptake rate is proportional to the cube of the wind speed. Gillette (1978a), in a wind tunnel test of the effects of sandblasting, wind speed, soil crusting, and soil surface texture on wind erosion, showed that the soil particle flux is proportional to the cube of the friction velocity ( $u_*$ ), where  $u_*$  is determined from the mean velocity profile over a horizontal surface,

$$U = \frac{u_*}{k} \ln \frac{z}{z_0}, \quad (2.1)$$

where  $U$  is wind speed at height  $z$ ,  $z_0$  is the surface roughness length, and  $k$  is von Karman's constant ( $\sim 0.4$ ). Blackwood and Wachter (1978) suggested that the storage pile emission rate,  $Q$  (mg/s), may be expressed as

$$Q = (cu^3 \rho_b^2 s^{0.345}) / (PE)^2, \quad (2.2)$$

where  $u$  is wind speed (m/s),  $\rho_b$  is bulk density (g/cm<sup>3</sup>),  $s$  is pile surface area (cm<sup>2</sup>),  $PE$  = Thornthwaite's precipitation-evaporation index (Thornthwaite, 1931), and  $c$  is a constant. Axetell (1978) suggested an emission factor of  $1.6u$  lb/acre-hr, where  $u$  is in m/s. Finally, wind erosion emissions from active storage piles may also be estimated from the EPA (1983) emission factor

$$EF = 1.9 [S/1.5] [(365-p)/235] [f/15], \quad (2.3)$$

where  $EF$  is the TSP emission factor (kg/day/hectare),  $S$  is silt content (% of particles < 75  $\mu$ m in diameter),  $p$  is number of days with > 0.25 mm precipitation per year, and  $f$  is the percentage of time that the unobstructed wind speed exceeds 5.4 m/s at the mean pile height. This equation is based on sampling emissions from sand and gravel storage piles and hence gives less accurate estimates when applied to other stored materials. It implies that no emissions occur when the unobstructed wind speed is less than 5.4 m/s.

Field tests with portable, open-floored wind tunnels indicated that threshold speeds, given in terms of threshold friction velocity ( $u_{*t}$ ), are typically 0.2 to 2 m/s depending upon the type of material (Gillette, 1978b; Gillette et al., 1980; and Cowherd et al., 1979). In

other field tests, threshold speeds of about 10 m/s at a height of 15 cm above a coal pile surface were estimated based upon the onset of visible particle uptake (Cowherd, 1982; Cuscino et al., 1983). Extrapolating these speeds to a 10 m reference height from the velocity profile (Equation 2.1) implies that very high mean wind speeds (e.g. 20 m/s) are needed for erosion at the surface ( $z=0$ ) to commence. Hence Cowherd (1982) suggested that strong wind gusts, not the mean wind, cause erosion, although it was noted that wind speeds 15 cm above a storage pile surface may approach the 10 m reference speed (Soo et al., 1981).

In the above relationships for particle uptake, emission rate is independent of time. However, unless an unlimited supply of erodible particles is present, erosion will be time dependent. Erosion rate has been observed to decrease with time (e.g. Cowherd et al., 1979). Cowherd (1982) suggested that erosion rate is proportional to the amount of erodible material remaining and that a given storage pile has an "erosion potential" equal to the total quantity of erodible material present on the surface prior to erosion. The erosion potential for coal increased with wind speed. An emission factor was then defined to be dependent upon the frequency of disturbance to the pile surface and the erosion potential at the expected wind gust speed.

A more comprehensive review of storage pile wind erosion emission factors may be found in Carrier and Neal (1984).

To summarize, particle uptake, hence storage pile emission rate, clearly depends upon the ambient wind speed. Previous studies indicate that uptake is highly sensitive to wind speed, being related either directly or to the cube of the speed, the threshold velocity, or only

occurring during high wind gusts. If the wind speed over a given area of a storage pile is reduced, then fugitive dust emissions from that area will also be reduced. The current study isolates the single variable, wind speed, as the primary factor affecting emission rates and attempts to evaluate the effectiveness of windbreaks in reducing particle uptake. A complete assessment, of course, would require an analysis of all factors, including material type, particle size distribution, moisture content, etc.

## 2.2 FLOW ABOUT WINDBREAKS

Rows of trees or hedges have been used to protect homes and agricultural fields from high winds for many years (e.g. Van Eimern, et al., 1964). Wind tunnel and field experiments have shown that windbreaks produce large areas of reduced wind speed in their lee. Speeds near the surface are typically reduced to half the upstream value for a distance of 8 to 12 windbreak heights downstream of a porous windbreak (e.g. Raine and Stevenson, 1977). Wind speeds are also reduced upstream of a porous windbreak. Perera (1981) observed reductions of 50% one windbreak height upstream.

Figure 2.1 shows typical streamline patterns for flow about solid and porous windbreaks. The streamline patterns are not drawn to scale; Caborn (1957) and Naegeli (1953) found that a "dense" barrier caused a sheltered region up to distances of 10-15h downwind and for a (50%) porous barrier, 20-25h. The general flow features are of interest here. Recirculation regions are evident both upwind and downwind of the solid windbreak; they are regions of low velocity and high turbulence intensity (Figure 2.1(a)). Air incident on the porous windbreak flows

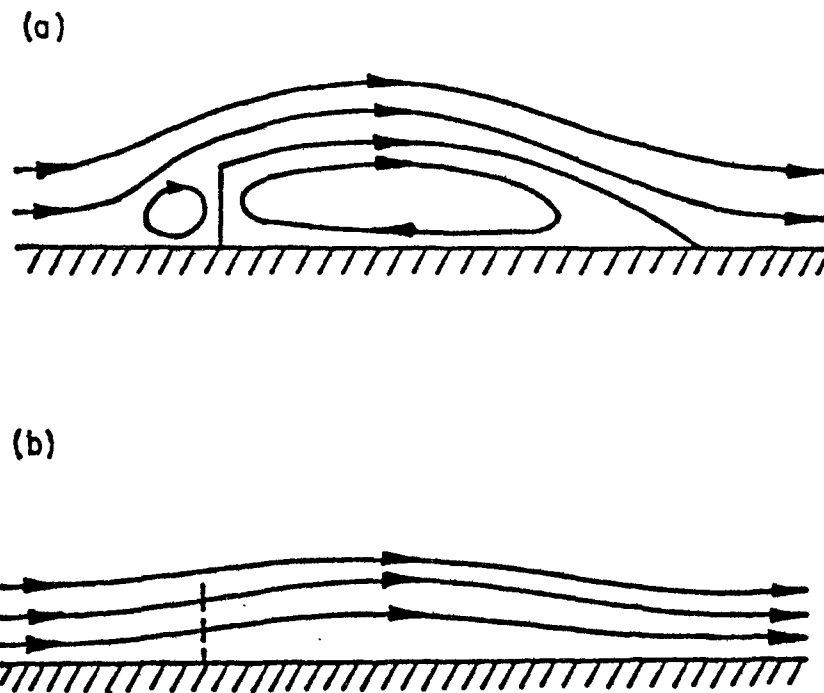


Figure 2.1 Sketches of streamlines about windbreaks: (a) solid, (b) porous.

over and through the windbreak. A region of reduced wind speed is evident in Figure 2.1(b); the upwind recirculation region is eliminated. In wind tunnel experiments, the low wind speed area moved downstream as porosity (ratio of open to total cross-sectional area) increased and, in general, at a given downwind distance, wind speed was less with a lower porosity windbreak (Raine and Stevenson, 1977). With the use of pulsed-wire anemometers which detect wind direction, other wind tunnel tests showed that as porosity increased, the downwind recirculation region became smaller and moved downstream (Perera, 1981).

Raine and Stevenson (1977) made several further observations. Greater wind speed reductions and turbulence intensity ( $u'/U$ , where  $u'$  is the r.m.s. longitudinal velocity fluctuation) enhancements were observed with decreasing porosity. But since the turbulent fluctuation at a given location varied much less with porosity than did the mean wind speed, the higher turbulence intensities were due to the lower  $U$ . The maximum in  $u'$  was located just above and extended downstream from the top of the windbreak. In the region bounded by the surface, the windbreak, and a line connecting the top of the windbreak to the surface just downstream of the velocity minimum ( $x \sim 8h$ , where  $h$  is windbreak height), the turbulent fluctuation  $u'$  was less than that observed in the absence of the windbreak, but above and downstream of this region,  $u'$  was greater, indicating the diffusion of turbulence generated in the windbreak-induced shear layer. Greater magnitudes and larger areas of wind speed reduction occurred with smoother upstream terrain and lower turbulence in the approach flow.

Perera (1981) also compared hot-wire (HWA) and pulsed-wire (PWA)

anemometer measurements downwind of a solid barrier. Velocity measured with the HWA was greater than that measured with the PWA for heights less than about  $1.8h$  at a downwind distance of  $5h$ , but at higher heights, the PWA measurements were greater. Longitudinal turbulence intensity from PWA measurements were greater than the HWA measurements at the downwind distance  $5h$  for heights up to  $4h$ , where they converged.

Effect of thermal stability was observed in a few field and wind tunnel studies. Seginer (1975a) observed that during unstable conditions, wind speed at  $z=0.25h$  beyond  $x=2.5h$  decreased with increasing stability. Between the porous windbreak and  $x=2.5h$ , stability was not important. Ogawa and Diosey (1980) observed that the length of the recirculating zone downstream of a solid fence was a maximum for near-neutral stability. It decreased rapidly as stability increased because the stable stratification inhibited changes in the flow caused by the fence. For unstable stratification, the length of the recirculating zone decreased slowly with increasing instability. Jacobs (1984) noted a faster recovery of wind speed with downwind distance for unstable stratification.

As expected, the location of the sheltered region shifts as the wind direction varies from that of the windbreak normal (Gandemer, 1981; Seginer, 1975b; Mulhearn and Bradley, 1977). Measurements along the windbreak normal showed that the minimum wind speed increases and its location moves toward the windbreak as the angle between the wind direction and the windbreak normal increased (Seginer, 1975a,b).

### 2.3 WINDBREAKS FOR STORAGE-PILE FUGITIVE-DUST CONTROL

Very little information on the use of windbreaks as a storage-pile

fugitive-dust control method is contained in the literature. Low efficiencies were reported by Bohn et al. (1978) and Jutze et al. (1977), 30% and "very low," respectively; although these were only estimates. No guidelines on windbreak design and use are available. Results of two laboratory investigations have been reported. Results of a water flume test indicated that the windbreak height should be at least  $1.4H$ , where  $H$  is the pile height and that the lower two-thirds of the windbreak be 20% porous and the remainder, 50% porous (Davies, 1980). However, the author did not state whether more than one windbreak height was used, nor which porosities were tested. Details of windbreak length with respect to the pile length and/or width and windbreak position were not given, nor were the details of the atmospheric boundary layer simulated. Results from a wind tunnel study using a two-dimensional windbreak and pile are reported by Soo et al. (1981) and Cai et al. (1983). Combinations of two windbreak heights ( $0.25H$  and  $0.5H$ ), two porosities (solid and 33% porous), and five positions (0, 1, 2, 3, and 4 pile heights from the pile base) were tested. The wind tunnel speed and model pile size were chosen to match the full-scale Reynolds number ( $Re=UL/v$ , where  $U$  and  $L$  are the characteristic wind speed and length, and  $v$  is kinematic viscosity), based on a pile height of 3.05 m and an ambient wind speed of 1.14 m/s. A 33% porous windbreak of height  $0.5H$ , placed the optimal distance of  $3H$  from the pile base reduced the wind speed by 50% just above the surface at the top of the windward face of the pile (Soo et al., 1981 and Cai et al., 1983). The position of  $2.5H$  was optimal for a 33% porous windbreak of height  $0.25H$  (Soo et al., 1981). Lower wind speeds

at the top of the windward face of the pile were observed with solid barriers of both heights at all the positions (Soo et al., 1981). In their study the atmospheric boundary layer was not simulated, although the flow was turbulent.

### 3. EXPERIMENTAL DESIGN AND INSTRUMENTATION

Some details of the wind tunnel boundary layer, the model piles and windbreaks and the experimental plan are given in the following subsections.

#### 3.1 EXPERIMENTAL DESIGN

The experiment was conducted in the EPA Fluid Modeling Facility (FMF) Meteorological Wind Tunnel (MWT), a low-speed, open-return tunnel having a test section 2.1 m high x 3.7 m wide x 18.3 m long. A complete description of the wind tunnel and operating characteristics can be found in Snyder (1979). Simulating the lower part of the atmospheric boundary layer (ABL) and determining model size and free-stream wind speed are necessary to assure that wind tunnel results will be valid for the full-scale case under investigation. A neutrally stratified simulated ABL was generated using a 153 mm high trip fence placed near the test section entrance. Gravel roughness composed of pebbles having typical diameters of 10 mm covered the tunnel floor downstream of the fence. The tunnel ceiling height was adjusted to achieve a zero longitudinal pressure gradient in the free stream. The velocity profile in the surface layer is described by Equation 2.1 and is shown in Figure 3.1. The tunnel free-stream speed was 4 m/s. Roughness length ( $z_0$ ) and friction velocity ( $u_{*}$ ) were determined from the log-wind law. The boundary layer was characterized by a depth of approximately 1 m, a  $z_0$  of 0.12 mm, and a  $u_{*}$  of  $0.048U_0$ , where  $U_0$  is the free-stream speed. Further details of the boundary layer are given by Castro and Snyder (1982).

Model size and free-stream wind speed should be determined from

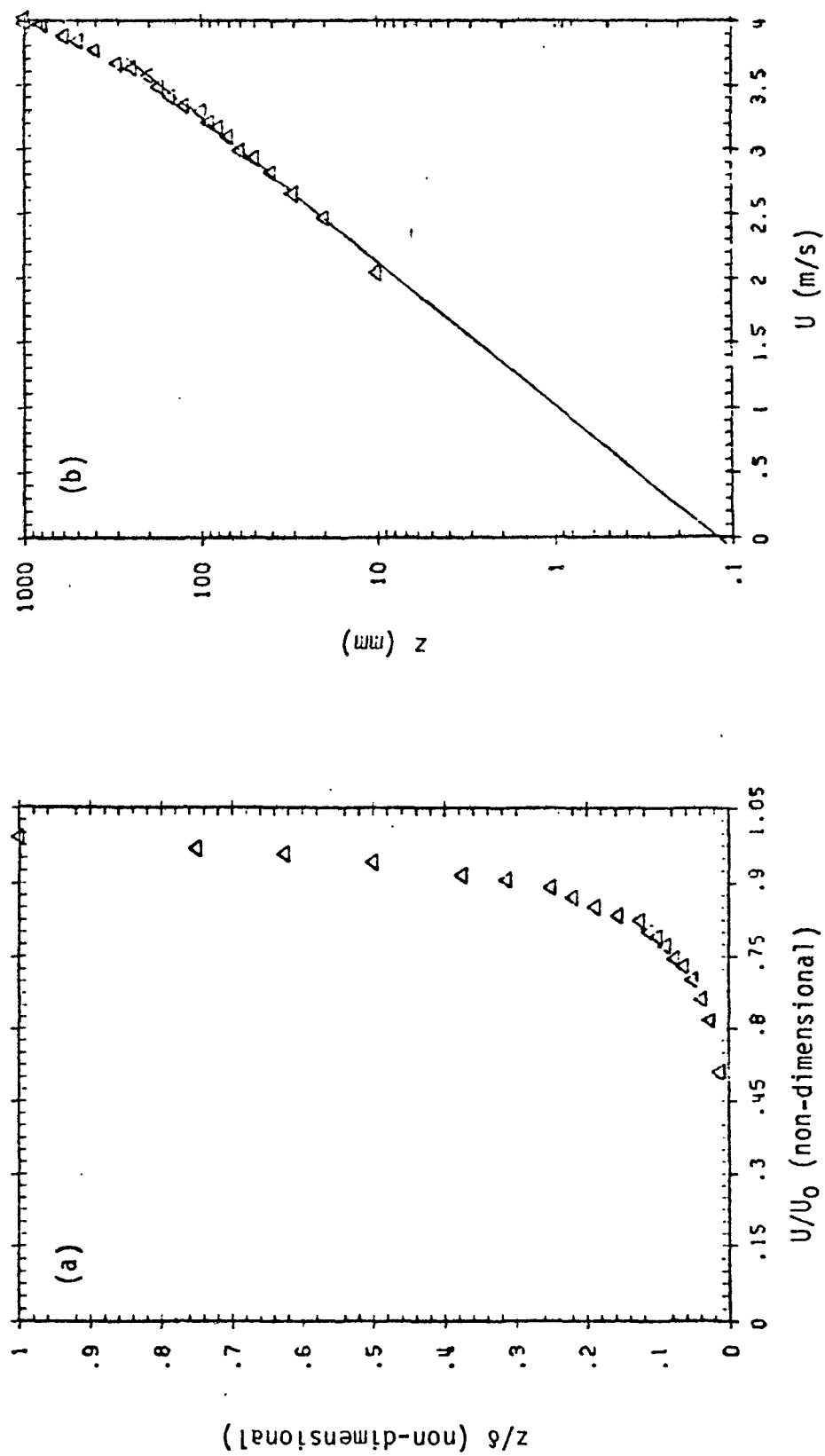


Figure 3.1 Boundary-layer velocity profile: (a) linear, (b) semi-logarithmic.

matching the model and full-scale Reynolds numbers. However, with typical scale reductions, the model  $Re$  is typically 3 to 4 orders of magnitude less than the full-scale  $Re$ . Very high wind speeds in the tunnel are generally required to match full-scale  $Re$ , but are often impractical. Fortunately for wind tunnel modeling, "geometrically similar flows are similar at all sufficiently high Reynolds numbers" (Townsend, 1956). That is, for  $Re$  greater than some minimum value, the turbulent flow structure described in terms of characteristic length and velocity scales is independent of  $Re$ . Since atmospheric flows are almost always aerodynamically rough (for all wind speeds), they are also  $Re$ -independent. Hence wind tunnel velocities, normalized by a reference speed, are equivalent to normalized full-scale values.

No two storage piles have the same shape and size, and active piles have constantly changing dimensions. For purposes of the present study, windbreak effects on two typical, but idealized, pile geometries are studied, with the results being generally applicable to many full-scale piles. Based on a survey of several coal piles at electric generating plants, typical piles are 11 m high, have slopes of  $37^\circ$  and range from conical to flat-topped in shape. The two piles modeled were an 11 m high conical pile with  $37^\circ$  slopes (base diameter 29.2 m) and an oval, flat-topped pile of height 11 m,  $37^\circ$  slopes, and base dimensions 63 m by 78 m (Figure 3.2). The larger pile is an elongated frustum. It is the lower part of a cone of base diameter 63.0 m and height 23.7 m, which is cut-off at 11.0 m, with a 15.0 m extension placed between the two halves of the frustum.

The model piles had to be small enough to be within the surface

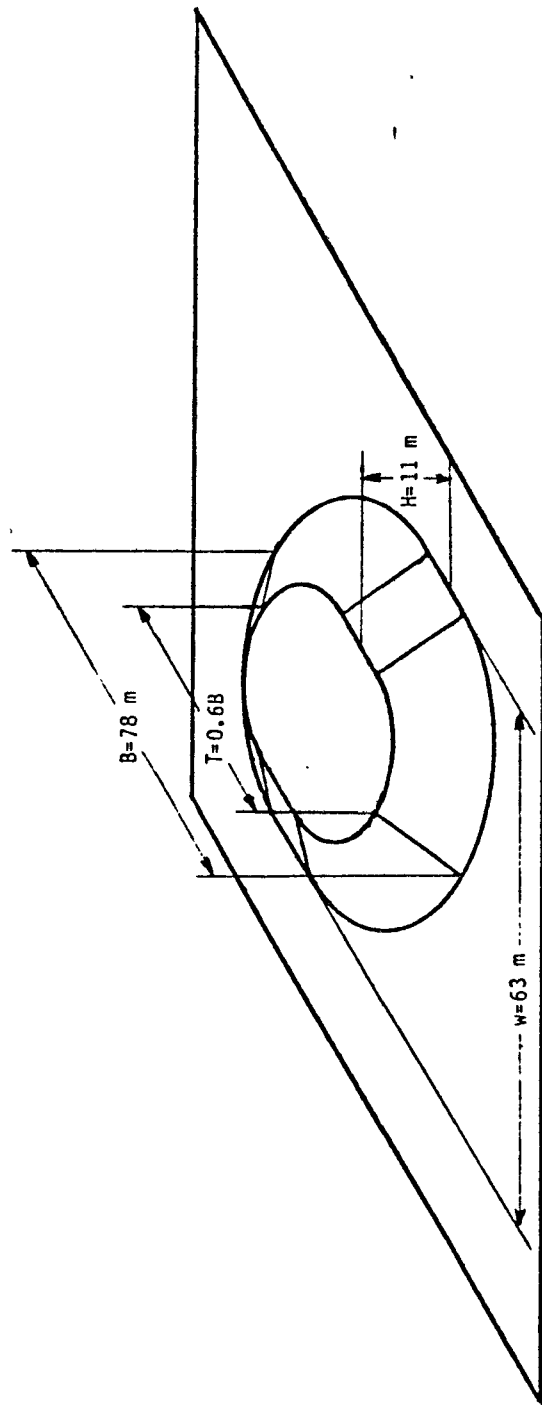


Figure 3.2 Sketch of oval, flat-topped pile.

layer but large enough to facilitate measurements and construction of windbreaks of height the same order as the pile height. A full-scale neutrally stratified ABL is typically 600 m high and has a surface layer depth of 100 m (Counihan, 1975). Since typical pile and windbreak heights are well within the surface layer, matching the ratio of the pile height to the boundary layer depth was not considered important. Instead, Jensen's (1958) criterion of matching the ratio of the model height to the surface roughness length ( $z_0$ ) was used to obtain the relevant model length scale. Model piles 110 mm high (1:100 scale) resulted ( $Re=2.9 \times 10^4$ , based on  $U_0$  and the pile height). The model surfaces were roughened to make them aerodynamically rough with roughness elements of size greater than approximately  $400\nu/U_0$  (roughness Reynolds number criterion) (Snyder, 1981). The pile could not be roughened with the same gravel as that covering the floor of the tunnel because the 10 mm gravel was considered too large for the pile size. Gravel having diameter less than 4 mm was used instead. With a free-stream speed of 4 m/s, the roughness Reynolds number criterion discussed above was met with the 4 mm gravel. The terrain surrounding actual piles is also usually rougher than the pile surface.

Finally, the windbreak material was chosen from 50%, 60%, and 70% porous synthetic material that is commercially available for use in windbreaks. The openings of 25 mm x 12 mm and 25 mm x 25 mm in the 60% and 70% porous screens were considered too large for the overall windbreak height (110mm) for direct use in the wind tunnel. Hence, a more uniform windbreak material having the same aerodynamic drag or pressure-drop coefficient as the more porous commercial screens was

desired. Caput el al. (1973) used the pressure-drop coefficient  $c_p$  to account for the porosity and size and shape of the windbreak openings. The pressure drop coefficient is defined as

$$c_p = \Delta P / (0.5 \rho U^2), \quad (3.1)$$

where  $\Delta P$  is the static pressure drop across the material,  $\rho$  is air density, and  $U$  is reference wind speed, here, the wind speed upstream of the windbreak.

The pressure drop coefficients of the three windbreak materials and a 16 x 18 mesh nylon screen (65% porous) were determined through tests in a smaller wind tunnel (1 m x 1 m x 4 m). The material was placed 1 m from the entrance to the test section and fully covered the cross section. The pressure drop was measured with pitot-static tubes placed upstream and downstream of the material, both connected to an MKS Baratron (Type 170M-6B) capacitance manometer. The output was digitized at a rate of 200 Hz over the 60 s sampling time, then processed on the EPA FMF Digital Equipment Corporation (DEC) PDP-11/40 minicomputer. The pressure drop coefficients for the 50%, 60%, and 70% porous materials and the mesh screen were found to be 5.5, 2.2, 1.4, and 1.8, respectively, independent of wind speed for  $U > 2$  m/s. The mesh screen was therefore used to represent the high porosity material as its  $c_p$  was midway between that of the 60% and 70% screens. Note that  $c_p$  for the 50% porous windbreak material is nearly three times that for the mesh screen.

Given the boundary layer, the model piles, and windbreak materials, the experimental procedure may be described. It consisted of three major parts:

(1) Measurement of surface wind speed patterns on a conical storage pile with and without a windbreak located upwind,

(2) Measurement of surface wind speed patterns on an oval, flat-topped pile with and without a windbreak located upwind or on the top of the pile, and

(3) Measurement of vertical profiles of velocity downstream of a porous windbreak over horizontal terrain.

The windbreak and conical pile set-up is shown in Figure 3.3. Each windbreak had vertical metal supports at both ends, which were tacked to the floor and to which guy wires were attached. The windbreak material was folded underneath the gravel-covered plywood sheets on the tunnel floor. Windbreaks of 50% and 65% porosity; heights  $0.5H$ ,  $1.0H$ , and  $1.5H$ , where  $H$  is the pile height; lengths  $1.0D$  and  $1.5D$ , where  $D$  is pile base diameter; and positions  $1H$  and  $3H$  from the upstream pile base were tested. All combinations of the parameters result in six windbreaks of each porosity placed at two different distances from the conical pile, i.e. a total of 24 cases (Table 3.1). Upon completion of these tests, one windbreak was placed at angles of  $20^\circ$  and  $40^\circ$  from the position normal to the incident flow.

For the oval, flat-topped pile, one of the windbreak orientations was similar to that shown in Figure 3.3; the longer axis of the pile being parallel to the windbreak. The same windbreak porosities and relative sizes and positions were used (the windbreak length is given in terms of the pile base length ( $B$ )) except that not all of the 24 cases were tested. A few other relative sizes were tested: heights  $0.75H$  and  $1.25H$ , and length  $0.6B$  (length of flat top, see Figure 3.2).

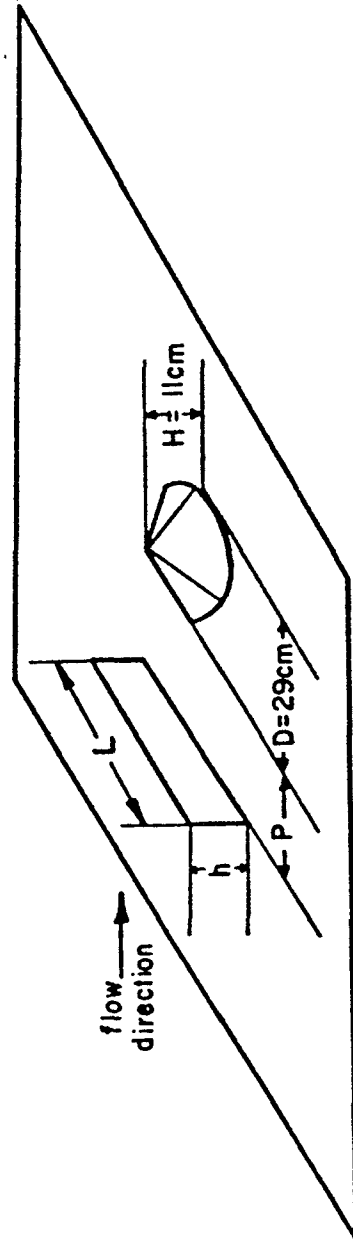


Figure 3.3 Geometry of conical pile and windbreak.

TABLE 3.1 COMBINATIONS OF WINDBREAK PARAMETERS USED WITH THE CONICAL PILE

porosity (%)	height (h/H)	length (L/D)	position (P/H)
50	0.5	1.0	1
50	0.5	1.0	3
50	0.5	1.5	1
50	0.5	1.5	3
50*	1.0	1.0	1
50	1.0	1.0	3
50	1.0	1.5	1
50	1.0	1.5	3
50	1.5	1.0	1
50	1.5	1.0	3
50	1.5	1.5	1
50	1.5	1.5	3
65	0.5	1.0	1
65	0.5	1.0	3
65	0.5	1.5	1
65	0.5	1.5	3
65	1.0	1.0	1
65	1.0	1.0	3
65	1.0	1.5	1
65	1.0	1.5	3
65	1.5	1.0	1
65	1.5	1.0	3
65	1.5	1.5	1
65	1.5	1.5	3

\*This windbreak was also placed 20° and 40° from the position normal to the incident flow.

The other windbreak orientation was to place a windbreak on the pile top to reduce wind speeds in active regions of the pile. The windbreaks were placed either close to the centerline or at the upstream edge of the pile top parallel to the pile's longer axis. Two heights,  $0.14H$  and  $0.27H$ , and two lengths,  $0.16T$  and  $0.5T$ , where  $T$  is the pile top length, were tested. For windbreaks in both positions the pile was rotated  $20^\circ$  and  $40^\circ$  to simulate other wind directions. The specifications for all the windbreaks used with the oval, flat-topped pile are given in Table 3.2.

The final phase of the project was to measure velocity downstream of the less porous windbreak oriented normal to the air flow to determine whether reverse flow was present and to relate the flow behind the windbreak to that over a pile placed in the lee of the windbreak. The windbreak chosen was 50% porous, 112 mm high and 1180 mm long (aspect ratio 10.5). Vertical profiles of velocity were measured with hot-wire and pulsed-wire anemometers along its centerline at downstream distances of 1, 5, 8, and 12 windbreak heights.

### 3.2 INSTRUMENTATION

Velocity profiles were measured at selected locations over the pile surface and flat tunnel floor with hot-wire and pulsed-wire anemometers and wind speeds were measured at a number of points over and close to the pile surface with fixed thermistors. Hot-wire and pulsed-wire probes were attached to the MWT instrument carriage which can position the probe to within  $\pm 1$  mm and may be operated by remote control outside the tunnel. The Cartesian coordinate system is oriented such that the  $x$ ,  $y$ , and  $z$  axes are longitudinal (positive downstream), lateral and

TABLE 3.2 COMBINATIONS OF WINDBREAK PARAMETERS USED WITH THE OVAL,  
FLAT-TOPPED PILE

porosity (%)	height (h/H)	length (L/B)	position (P/H)
50	0.5	0.6	1
50	0.5	0.6	3
50	0.5	1.0	1
50	0.5	1.0	3
50	0.5	1.5	1
50	0.75	1.0	1
50	0.75	1.0	3
50	1.0	0.6	1
50	1.0	0.6	3
50	1.0	1.0	1
50	1.0	1.0	3
50	1.0	1.5	1
50	1.25	1.0	1
50	1.25	1.0	3
50	1.5	0.6	1
50	1.5	0.6	3
50	1.5	1.0	1
50	1.5	1.0	3
50	1.5	1.5	1
65	0.5	0.6	1
65	0.5	0.6	3
65	0.5	1.0	1
65	1.0	0.6	1
65	1.0	0.6	3
65	1.0	1.0	1
65	1.0	1.0	3
65	1.5	0.6	1
65	1.5	0.6	3
65	1.5	1.0	1
		length (L/T)	location
65*	0.14	0.5	upstream edge
65*	0.14	0.5	centerline
65	0.27	0.16	upstream edge
65	0.27	0.5	upstream edge
65	0.27	0.5	centerline

\*These windbreaks were also placed 20° and 40° from the position normal to the incident flow.

vertical, respectively. The corresponding velocity components are  $u$ ,  $v$ , and  $w$ . Theory and operation of the three anemometers will be briefly discussed.

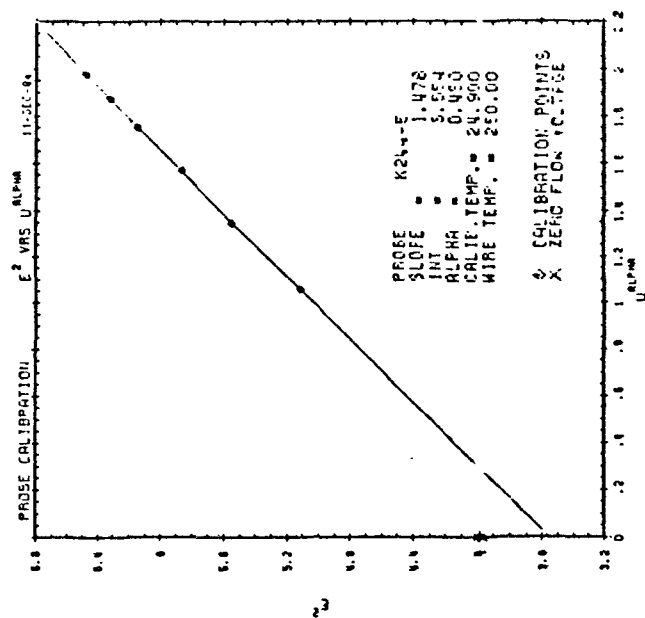
Hot-wire anemometers are commonly used in turbulent, wind tunnel flows. A TSI, Inc. constant temperature hot-wire anemometer (model 1053B) with a TSI boundary-layer cross-wire probe (model 1243) was used to obtain vertical profiles in the undisturbed (no pile, no windbreak) boundary layer and downstream of a windbreak. Mean velocity, angle of flow, r.m.s. turbulence velocities and turbulence intensities in two directions (longitudinal and vertical) and Reynolds stress were obtained. Yaw response corrections developed by Lawson and Britter (1983) were applied to the turbulence intensity and stress measurements. The anemometer has been extensively used by other investigators at the EPA FMF (e.g., Castro and Snyder, 1982; Pendergrass and Arya, 1984). The probe was calibrated in the free stream against a standard pitot-static tube each day. The hot-wire output was fit to a King's law form by the hot-wire calibration routine CALLPA:

$$E^2 = aU^\alpha + b, \quad (3.2)$$

where  $E$  is output voltage,  $U$  is wind speed, and  $a$ ,  $b$  and  $\alpha$  are constants. CALLPA gives the best-fit  $a$ ,  $b$ , and  $\alpha$ . An example of the computer output is shown in Figure 3.4. The hot-wire output was digitized to 12 bit precision and processed at a rate of 500 Hz on the PDP-11/40 with the program HOT. 90 s samples provided reasonably repeatable results.

The pulsed-wire anemometer is used to measure mean and fluctuating velocities in regions where turbulence intensity is very high or flow

CHANNEL \* 6  
ALPHA=0.45 SLOPE=1.4776 INT.=3.5527  
X Y (MEAS) Y (CAL) TDEV (Z) UDEV (V)  
1.059 5.117 5.118 0.0104 -0.0705  
1.348 5.548 5.545 -0.0529 -0.1110  
1.570 5.866 5.873 0.1203 -0.6318  
1.751 6.148 6.141 -0.1181 -0.5958  
1.876 6.324 6.325 0.0185 -0.0023  
1.981 6.479 6.461 0.0225 -0.1027  
UDEV\*\*2 SUM=0.8268E+00



CHANNEL \* 6  
ALPHA=0.48 SLOPE=1.4776 INT.=3.5527  
X Y (MEAS) Y (CAL) TDEV (Z) UDEV (V)  
1.059 5.117 5.118 0.0104 -0.0705  
1.348 5.548 5.545 -0.0529 -0.1110  
1.570 5.866 5.873 0.1203 -0.6318  
1.751 6.148 6.141 -0.1181 -0.5958  
1.876 6.324 6.325 0.0185 -0.0023  
1.981 6.479 6.461 0.0225 -0.1027  
UDEV\*\*2 SUM=0.8268E+00

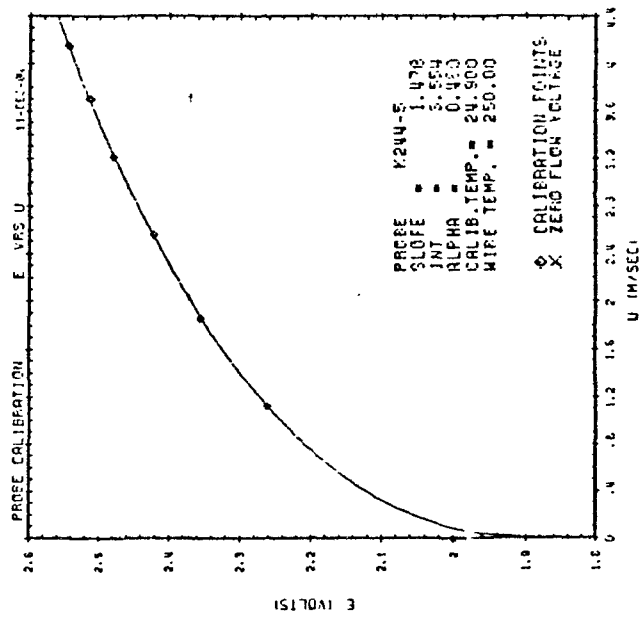


Figure 3.4 Example hot-wire anemometer calibration plots.

reversal occurs. Measurements with the pulsed-wire anemometer were taken downstream of a windbreak since flow visualization indicated intermittent flow reversal.

A pulsed-wire probe consists of a pulsed wire normal to and between two parallel sensor wires (Figure 3.5). The pulsed wire is activated by a voltage pulse, momentarily raising the pulsed-wire temperature to several hundred degrees Celcius and heating the air surrounding the wire. The heat, acting as a tracer, is advected by the wind with the velocity occurring at that instant. Depending on the instantaneous flow direction, one of the two sensor wires (operated as resistance thermometers) senses the tracer. Thus, the basic measurement is of the time-of-flight of the heat tracer from the pulsed wire to either of the sensor wires. Ideally, the time-of-flight  $t$  is

$$t = d/(U \cos \gamma), \quad (3.3)$$

where  $d$  is the distance between the pulsed wire and sensor wire,  $U$  is the magnitude of the velocity vector and  $\gamma$  is the angle between the direction normal to the probe plane and the instantaneous velocity vector (Figure 3.5). The probe plane is the plane parallel to all three wires. In other words, given the separation distance between the wires, the velocity component normal to the probe plane is calculated from the time-of-flight. If the velocity at the time of pulsing is close to zero or if the angle of flow ( $\gamma$ ) is greater than about  $70^\circ$  (based on the sensor wire length and  $d$ ), the heat tracer will not be sensed at the sensor wires. In such cases, the velocity is recorded as zero. For operation in turbulent flow the wire is pulsed many times per second over a given time period to obtain repeatable mean and

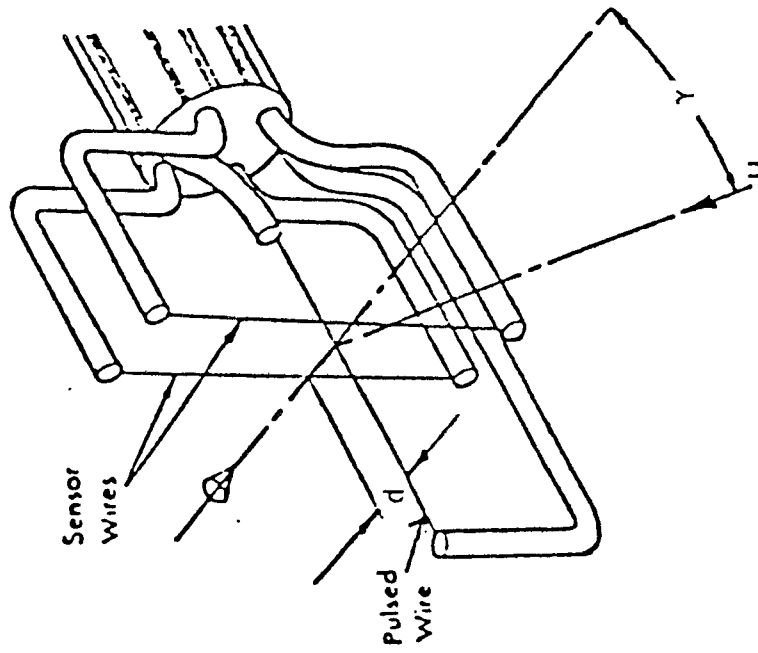


Figure 3.5 Sketch of a pulsed-wire anemometer probe.

r.m.s. fluctuating velocity components.

The basic electronic components, in addition to the sensor wires, are a differential amplifier, a differentiator, and two comparators. The polarity of the output from the differential amplifier indicates which sensor wire received the tracer. The signal is then differentiated to provide a more clear indication of the time the heat tracer was sensed since the tracer diffuses as it is advected. One comparator is set to be triggered by a positive sensor wire signal (positive velocity) and the other by a negative signal (negative velocity). A 12 bit binary counter begins when the pulse is fired and stops when either of the comparators is triggered. Hence the time-of-flight is measured and the flow direction is known. The other major electronic component is a circuit to eliminate the spike on the sensor wire circuit which occurs when the pulse is fired. The sensor signals at various stages of the electrical operation may be observed on an oscilloscope. Typical signals are shown in Figure 3.6; the signal with the spike, the signal less spike, the differentiated signal, and the time-of-flight signal. The time-of-flight signal indicates when the counter stops. Further details on the theory of the pulsed-wire anemometer are found in Bradbury and Castro (1971).

A PELA Flow Instruments, Ltd. pulsed-wire anemometer was calibrated in the tunnel free stream against a standard pitot-static tube. The probe plane was oriented perpendicular to the velocity component of interest,  $U$ . The FMF pulsed-wire calibration computer program PWCAL fits the wind speed,  $U$ , and time-of-flight,  $t$ , data to the relation

$$U = C/t + F/t^2 \quad (3.4)$$

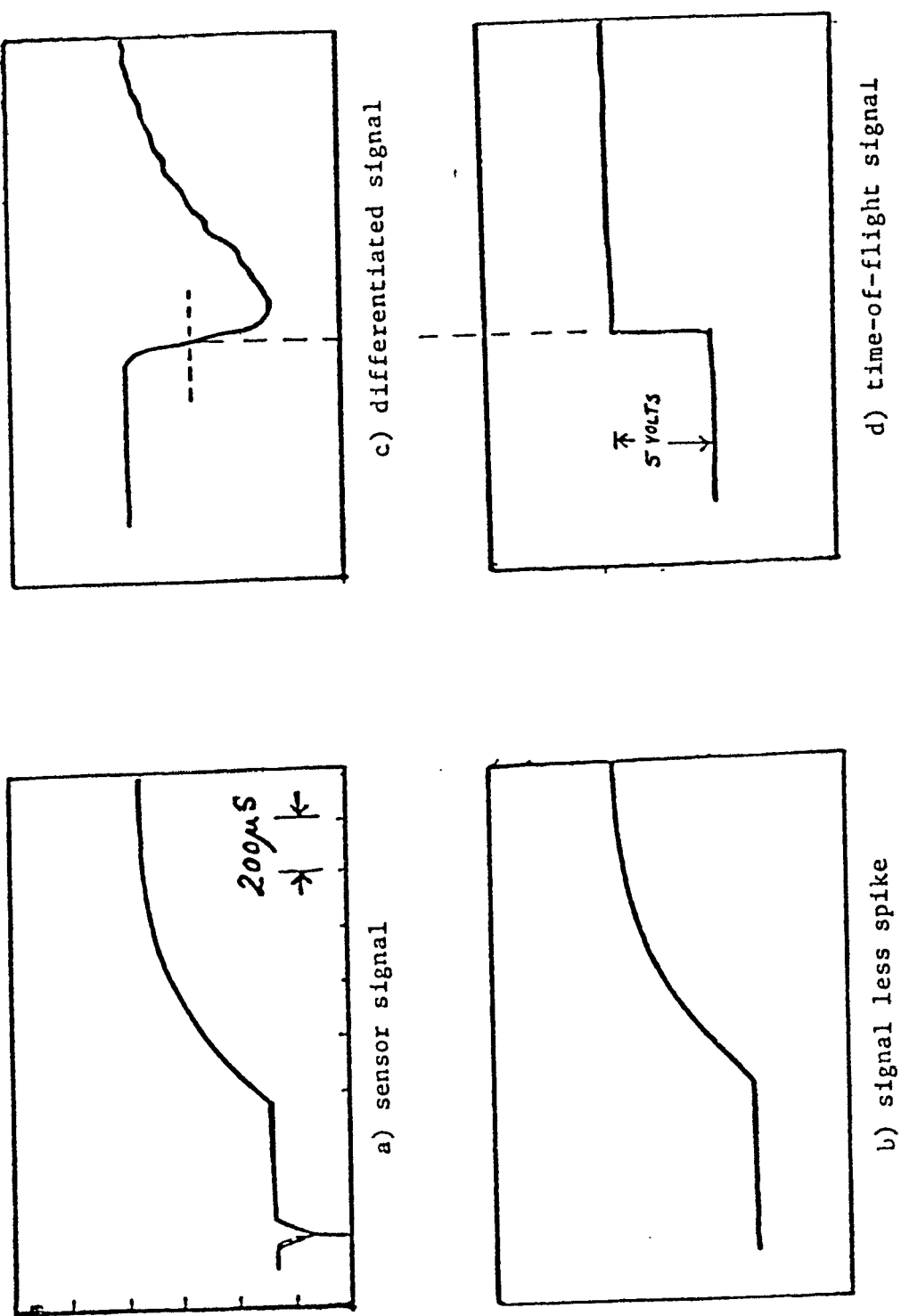


Figure 3.6 Typical signals observed from various stages of the pulsed-wire anemometer.

where C and F are constants. An example of the fit is shown in Figure 3.7. After one sensor wire was calibrated, the probe was rotated 180° to calibrate the other sensor wire. Data were collected and processed by the program PWAHOT on the FMF' DEC PDP-11/44. A sampling rate of 20 Hz over 3 minutes gave reasonably repeatable results.

The last instrument to be described is the thermistor which was used to measure wind speeds near the pile surface at various locations. We have considered wind speed near the surface as the basic parameter affecting particle uptake. Unfortunately, it is difficult to measure the wind speed near a roughened, sloping surface, particularly when the wind direction at the measurement point is unknown and difficult to determine. Pitot-static tubes and hot-wire anemometers require certain orientation with respect to the wind for accurate results. Heated thermistor beads were used here for several reasons. First, several thermistors could be mounted on the pile surface, eliminating the tedious task of moving a hot-wire from location to location, orienting it properly and placing it the same distance from the surface for each sample. Once the thermistor was fixed at the pile surface, errors resulting from differences of thermistor orientation and height, and effects of local roughness elements were minimized by comparing wind speed at a specific point on the pile for the cases with and without a windbreak.

The resistance-temperature relationship for thermistors is expressed as

$$R = R' \exp \{ \beta [ (T)^{-1} - (T')^{-1} ] \}, \quad (3.5)$$

where R and R' are the resistances at temperatures T and T',

14-000-04

PROBE Pnppp PSS  
 TAIG LEVELS= 1. 1. SW CURRENT=2. SW DRIN=4. Pn VOLT= 6.  
 $U = 1764.05/T + 0.9522 \cdot 10^5 / T^2$   

1/T	U (MERC)	U (C)	U (S) %
0.00159	4.470	4.453	-0.372
0.00146	3.873	4.002	0.605
0.00130	3.420	3.423	0.005
0.00112	2.850	2.822	-0.977
0.00096	2.310	2.310	-0.021
0.00079	1.800	1.816	0.908
0.00058	1.270	1.237	-2.559
0.00034	0.630	0.673	6.309

SSE = 0.00499 R = 0.9993

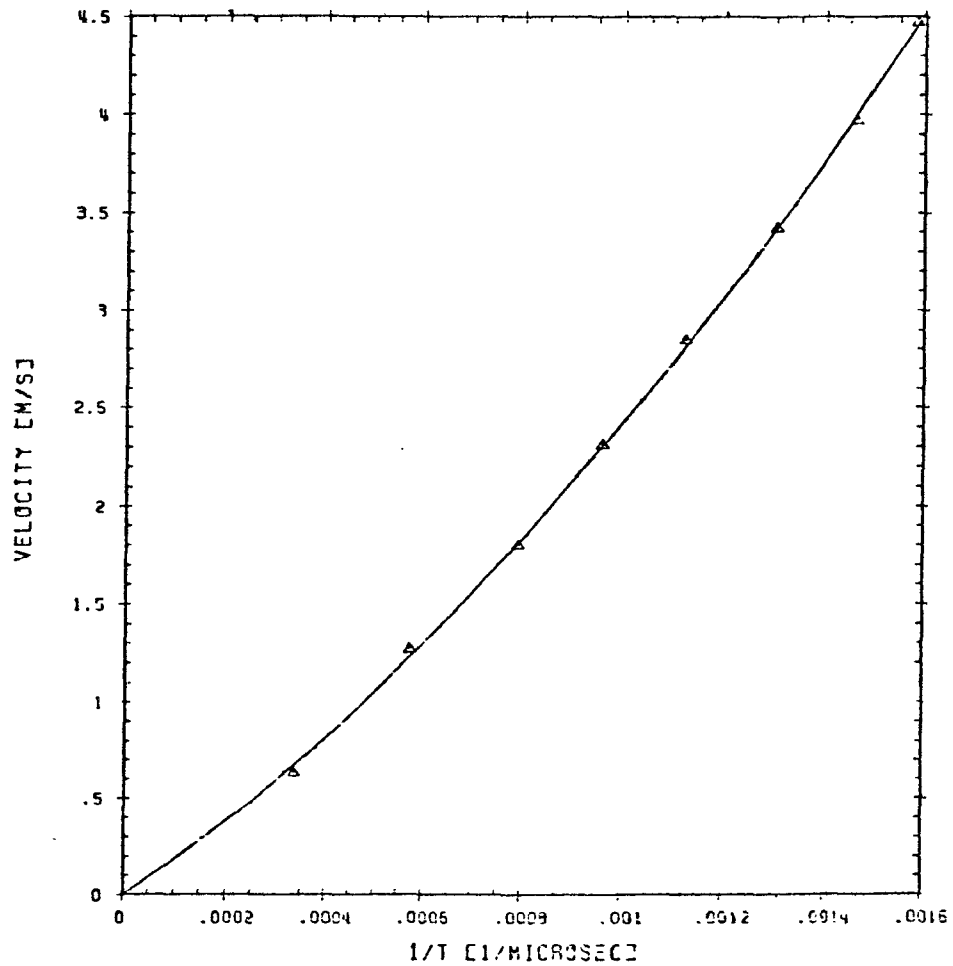


Figure 3.7 Example pulsed-wire anemometer calibration plot.

respectively, and  $\beta$  is a constant dependent on the thermistor material. All the thermistors (Fenwal GB31J1) were calibrated in a hot oil bath. Calibration curves for two of those calibrated and the Fenwal rated curve,  $R(25^\circ\text{C}) = 1000 \pm 200 \, \Omega$ ,  $\beta = 3442 \pm 90 \, \text{K}$ , are shown in Figure 3.8. Fenwal specified the thermistor time constant of 4 s in still air at  $25^\circ\text{C}$ . The thermistor diameters were about 1 mm and their lengths were about 1.5 mm.

The electric circuit consisted of a regulated power supply of constant voltage  $E$  and thermistor-resistor pairs in parallel with the power supply (Figure 3.9). The voltage across each series resistor is the output voltage ( $V_i$ ). Voltages  $V_i$  and  $E$  were digitized at a rate of 50 Hz and processed on the PDP 11/40 minicomputer with the computer program THE. A one minute sampling time gave reasonably repeatable results.

Thermistor anemometers operate under the same basic principle as do hot-wire anemometers, that is, the heat loss from the sensor is a function of wind speed. Rasmussen (1962) has shown that

$$i^2 R = K(T_T - T_a), \quad (3.6)$$

where  $i$  is current through the thermistor,  $R$  is thermistor resistance,  $T_T$  and  $T_a$  are thermistor and ambient temperature, respectively, and  $K$  is the dissipation factor.  $K$  is a function of the wind speed and the properties of the fluid surrounding the thermistor, and was determined experimentally as follows. The thermistor was placed in the center of the smaller wind tunnel with the probe support body and the thermistor oriented vertically (the same orientation with respect to the air flow as for a thermistor mounted on the model pile). At each wind speed,  $E$

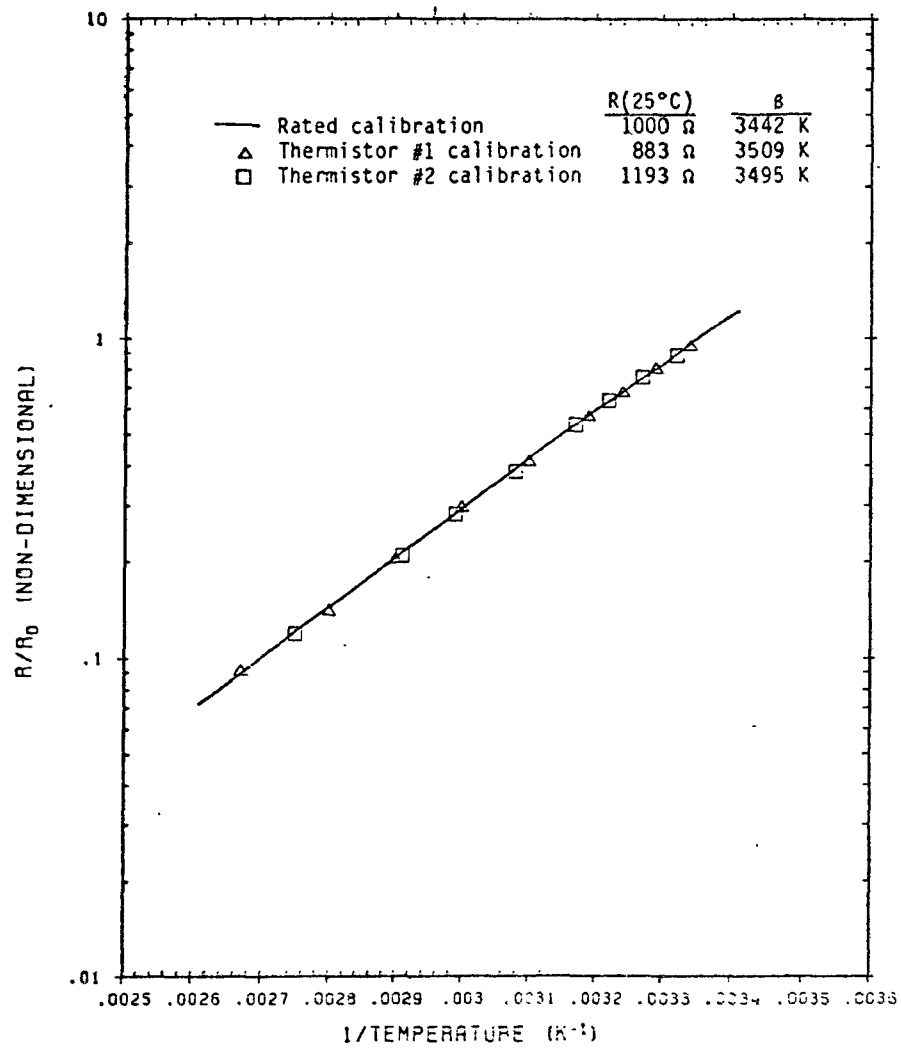


Figure 3.8 Resistance-temperature thermistor curves.

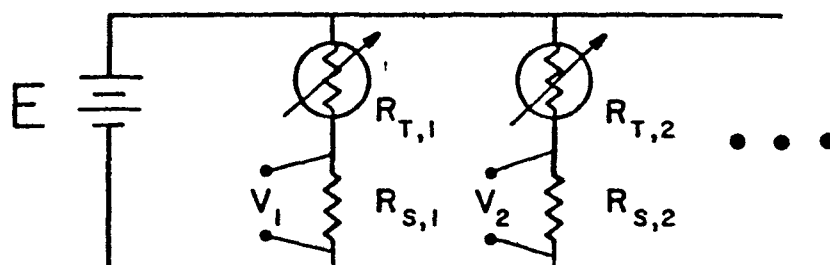


Figure 3.9 Thermistor circuit.

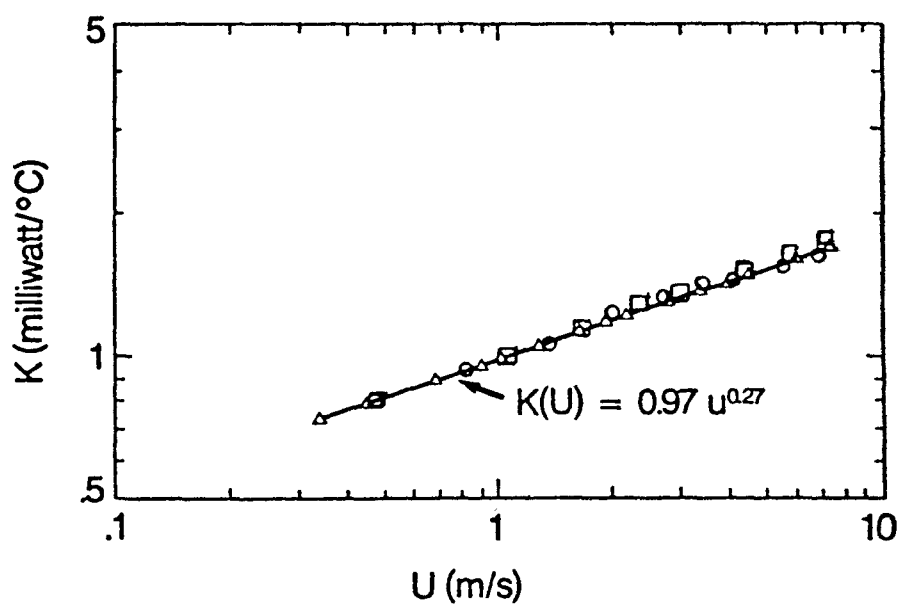


Figure 3.10 Dissipation factor vs. wind speed for Fenwal GB31J1 thermistors. Triangles: original data. Squares and circles: additional data.

and  $V_i$  were measured. From those,  $i$ ,  $R$  and  $T_T$  were calculated.  $T_a$  was measured with a YSI model 4320 temperature sensor. Hence,  $K$  at each wind speed was calculated. By varying the wind speed from 0.3 m/s to 8 m/s, the functional relationship of  $K$  (mW/°C) to  $u$  (m/s) was found to be (Figure 3.10)

$$K = 0.97u^{0.27}. \quad (3.7)$$

Hence, thermistor output is related to wind speed. It was originally assumed that this relationship was valid for all the thermistors used in this project. Later, two other thermistors were similarly calibrated. The curves of thermistor output ( $K$ ) vs. tunnel wind speed were similar to that of the original curve (refer to Figure 3.10); the maximum differences in wind speed were  $\pm 10\%$ . The original calibration tended to slightly overestimate wind speed as compared to the data from the other thermistors.

Tests of thermistor sensitivity to orientation were also conducted in the smaller wind tunnel. With the probe and support in the vertical position, two tests were conducted. First, the probe was rotated about the vertical axis, sampling the output for several orientations at a given wind speed. The maximum difference in measured wind speed from the tunnel speed was 5%. Second, the wind speed calibration was made with the probe oriented vertically as described above, but rotated 90°, to observe effects of the leads exposed between the thermistor and the support. Measured speeds were within the scatter of the calibrations for the probe in the original orientation. Hence, orientation about the vertical axis was not significant. Yaw sensitivity was tested by orienting the probe and support in the horizontal, normal to the air

flow, and rotating the support in the xy-plane to angles up to  $\pm 30^\circ$ . The maximum difference in measured wind speed from the tunnel speed was 8%.

The thermistors were mounted normal to and about 2 to 3 mm above the pile surfaces; close enough to the surface that the flow presumably parallels the surface, and where wind speed may be assumed to be directly related to the surface shear stress. Nine thermistors were mounted at different elevations on the conical pile in the arrangement shown in Figure 3.11. 81 thermistors were mounted on the oval, flat-topped pile in the arrangement shown in Figure 3.12.

Thermistor and hot-wire anemometer (TSI Model 1210, end-flow single-wire) measurements were compared to further substantiate thermistor use as an anemometer and the use of Eq. 3.7. For the pile oriented in the position shown in Figure 3.11 with air flow from the left, wind speeds were measured by the middle thermistor on the windward side of the pile. Wind speeds were calculated with the calibration equation (Eq. 3.7) for several wind tunnel tachometer settings. The pile was rotated approximately  $45^\circ$  and the hot-wire was placed at the same relative position as the thermistor. Wind speeds were measured at the same tachometer settings. The results showed good agreement (Figure 3.13). However, slight differences in height above the surface, individual roughness elements, and thermistor and hot-wire orientation could cause larger differences in the velocities measured by the two probes. The same may be expected for velocity measurements using different thermistor probes in apparently similar settings.

As discussed above, the maximum error in wind speed due to

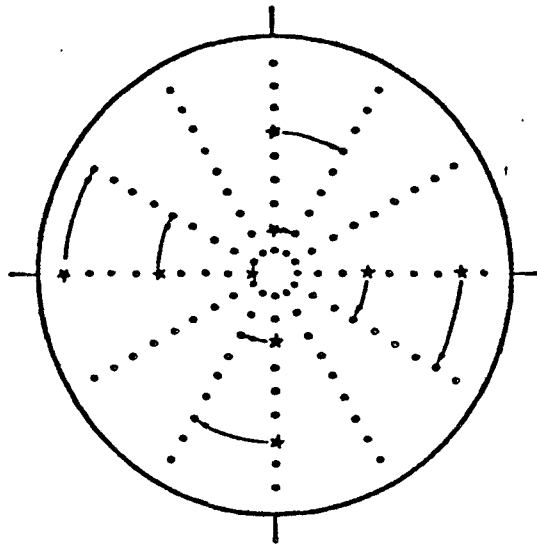


Figure 3.11 Top view of conical pile. Stars: Thermistor positions on pile. Dots: Effective thermistor positions due to pile rotation.

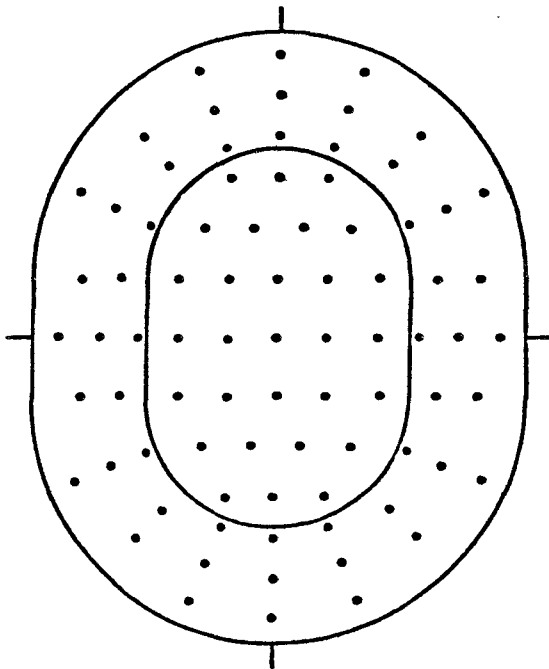


Figure 3.12 Top view of oval, flat-topped pile. Dots: Thermistor positions.

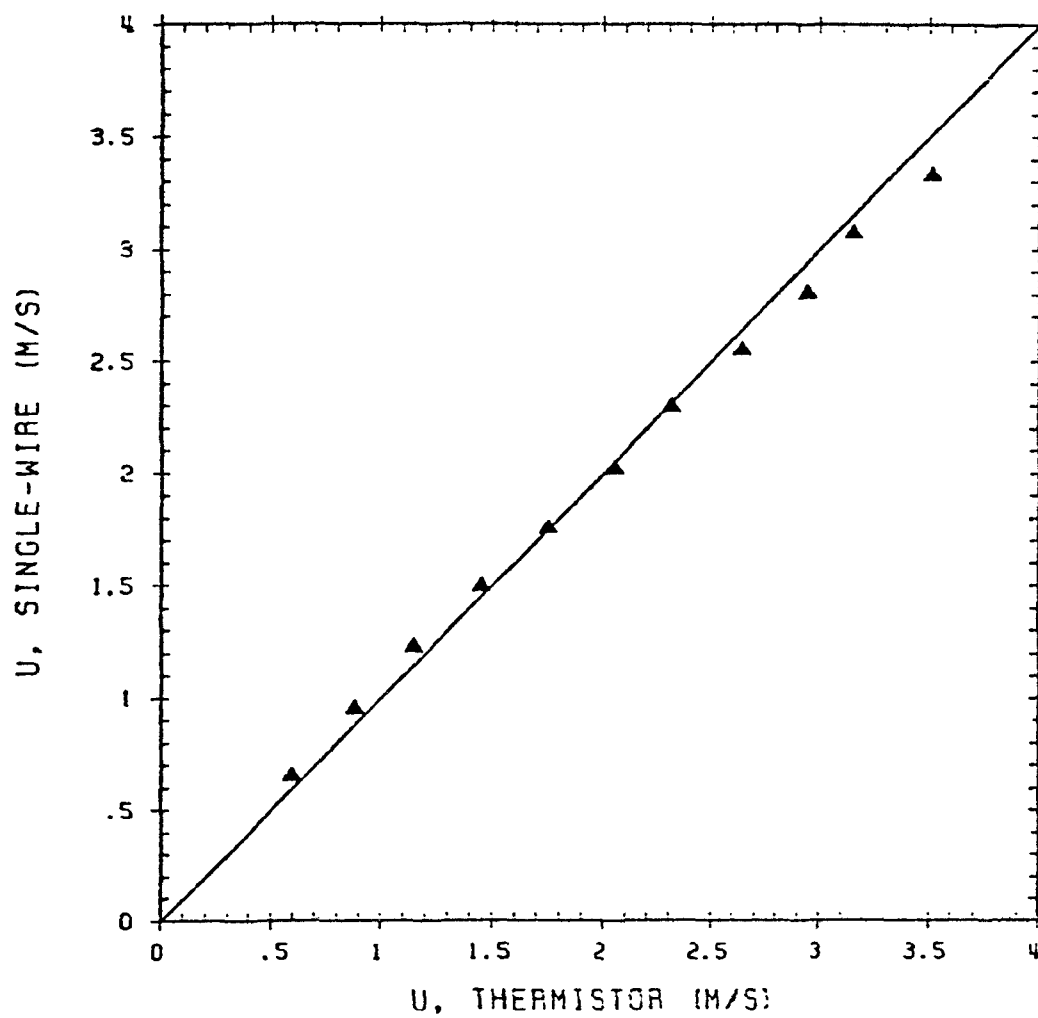


Figure 3.13 Comparison of thermistor and single-wire wind speed measurements.

thermistor orientation was  $\pm 8\%$ . Possible systematic errors resulting from the application of the calibration curve (Eq. 3.7) to all the thermistors could have been eliminated if each thermistor had been calibrated; however, due to time constraints, each probe could not be calibrated. Effects of individual roughness elements and thermistor height above the surface were other possible sources of systematic error. For the purposes of the present study, wind speed was used more as a relative, than absolute, measure, i.e. wind speed with and without a windbreak or wind speed with one windbreak and that with another were compared. The error indicated above is for absolute wind speed, but relative wind speed was of more importance here; its error was expected to be even less.

In addition, thermistors cannot detect flow reversal, i.e. they respond to wind speed and not wind velocity. If reverse flow were steady, the magnitude of the measured wind speed would be fairly accurate. On the lee side of the piles, with unsteady flow, the measured average mean wind speed will be higher than the actual (vector-averaged) speed.

Wind speed distributions were measured on the piles in the absence of any windbreak at least once every three days and frequently once a day to determine system repeatability. The peak-to-peak difference at a given position was  $\pm 10\%$ , an r.m.s. error of  $\pm 2\%$ , indicating quite good repeatability.

For the conical pile, each run consisted of measuring the wind speed with the nine thermistors, rotating the pile  $30^\circ$ , measuring the wind speed at these nine positions, etc., through  $360^\circ$ , resulting in

108 data points per run (refer to Figure 3.11). For the oval, flat-topped pile, each run consisted of measuring the wind speed at the 81 positions shown in Figure 3.12.

#### 4. FLOW ABOUT A POROUS WINDBREAK

Mean and fluctuating longitudinal velocity components were measured downstream of a representative windbreak (50% porous, height  $(h)=112$  mm, aspect ratio=10.5) with hot-wire (HWA) and pulsed-wire (PWA) anemometers to quantitatively describe the flow structure in the sheltered area, to determine if flow reversal occurred, and to further explain results of the major part of the project. Due to the finite size of the windbreak, the flow was expected to be three-dimensional. Vertical profiles were taken at distances of 1, 5, 8, and 12h from the windbreak. The results from the two anemometers may also be compared.

"Streamlines" for two-dimensional, steady flow were obtained from the FMF computer program STRFUN which calculates the height at which a given stream function value ( $\psi$ ) occurred ( $\psi = \int u dz$ ). Since the flow was likely three-dimensional, the calculated "streamlines" are not necessarily the true streamlines; knowledge of the three velocity components are required to calculate the true streamlines. However, along the centerline not too far from and close to the windbreak, the flow is expected to be nearly two-dimensional. "Streamlines" derived from the pulsed-wire data are shown in Figure 4.1. The PWA data was used because it was expected to be more accurate since the PWA senses flow reversal. Note the similarity to Figure 2.1(b). A region of low wind speed near the surface between 2h and 8h from the windbreak is evident, with the air flowing up and over this region. Flow visualization indicated intermittent flow reversal (unsteady flow) near the surface in this region. Effects of the windbreak are noticeable up to  $z=4h$ , with upward deflection apparent as far downstream as  $x=6h$ .

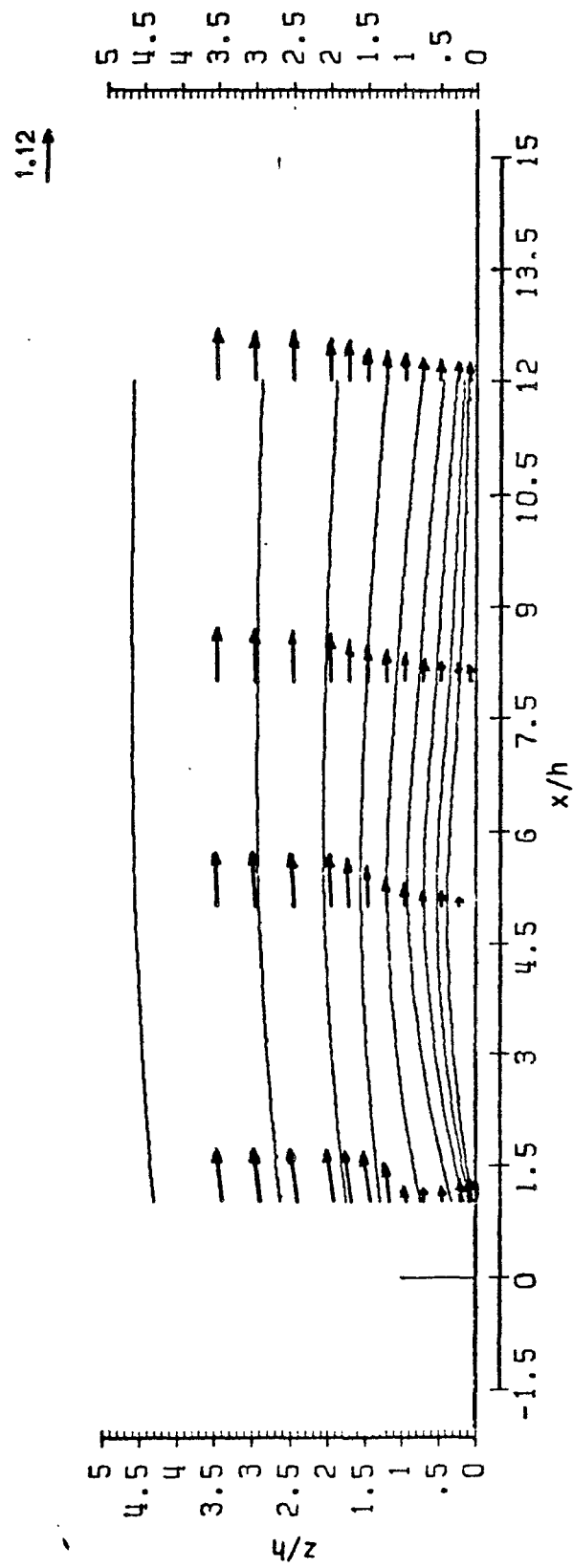


Figure 4.1 "Streamlines" and normalized velocity vectors downstream of a porous windbreak.

For steady flows, velocity vectors are parallel to streamlines. Since the flow angle in the  $xz$ -plane was given by the hot-wire output, the normalized velocity vectors ( $U/U_R(h)$ ) are also shown in Figure 4.1 ( $U_R(h)$  is the wind speed at the windbreak height, but in its absence). The flow generally parallels the "streamlines" except in the region below the windbreak height at  $x=1h$ , suggesting that the flow is three-dimensional, i.e. that some flow in the lateral direction exists, even along the centerline. Vortices may be formed as the air flows round the sides of the windbreak. The hot-wire observed angles are not nearly as large as those implied by the "streamlines" (derived from PWA data) because of differences in wind speed profiles measured by the two instruments. The angles clearly show upward flow at  $x=1h$  and downward flow at  $x=8h$ .

Relative wind speed deficit may be defined as  $[U_R(z)-U(z)]/U_R(z)$  where  $U_R(z)$  is the reference speed (measured with the HWA) at the location of the windbreak but in its absence and  $U(z)$  is a speed (measured with the PWA) at some distance downstream of the windbreak. Again, PWA data are presented as they are expected to be more accurate. Lines of constant relative deficit are seen in Figure 4.2. Downstream distance and height are scaled by the windbreak height  $h$ . A large region of wind speed reduction was observed downstream of the windbreak. The height of the region increased from  $z \approx 1.4h$  at  $x=1h$  to  $z \approx 3h$  at  $x=12h$ . Below  $z=1h$ , wind speeds were reduced at least 50% from the upstream value at the same height. The greatest deficits were observed for heights less than  $z=0.5h$  between approximately 4 and 8h downstream. In other words, the maximum deficit did not occur immediately downstream

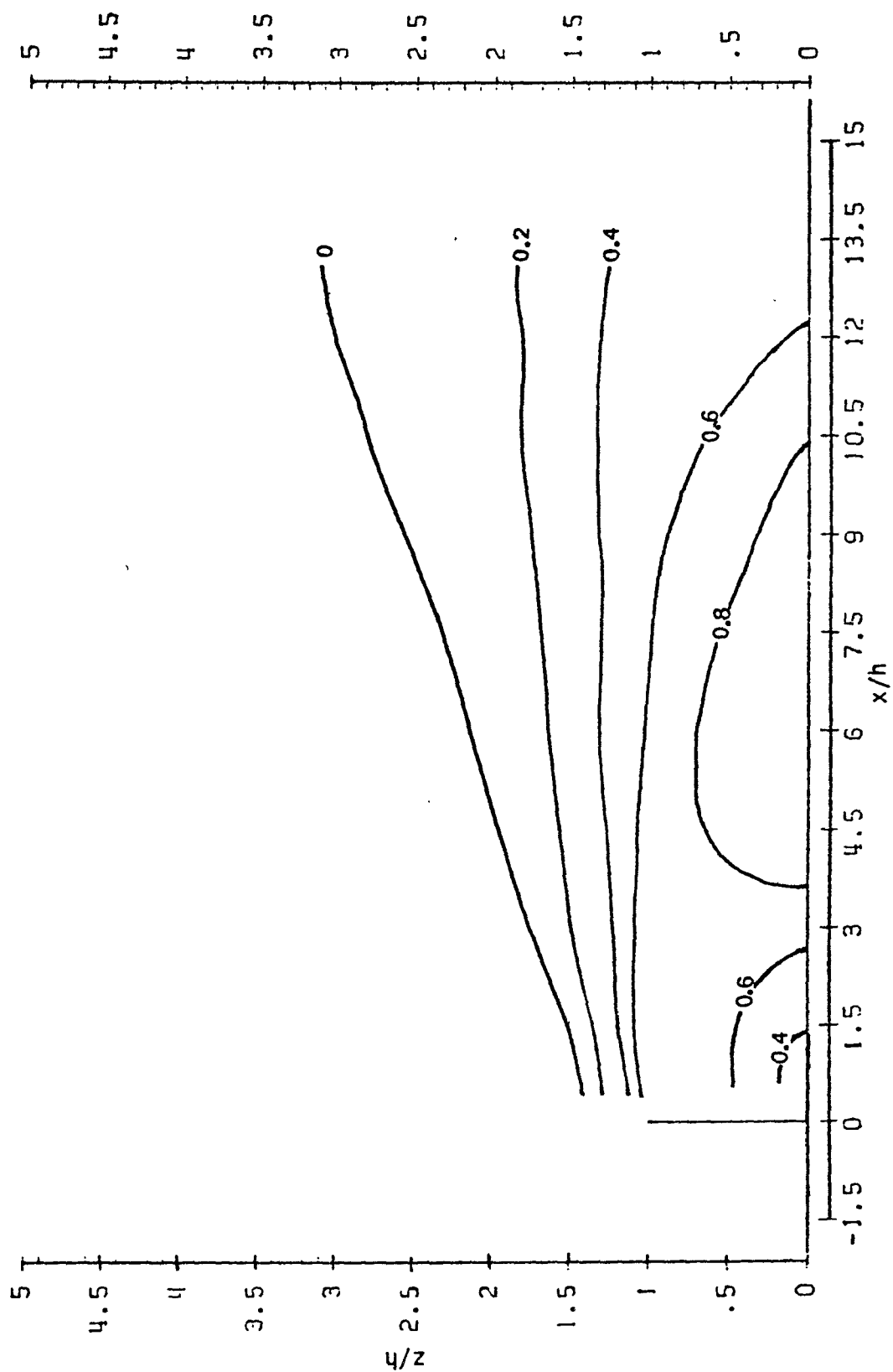


Figure 4.2 Relative wind speed deficit downstream of a porous windbreak.

of the windbreak, but occurred farther downstream. A strong gradient is clearly evident just above and downstream of the windbreak.

Lines of constant turbulence intensity are shown in Figure 4.3, where turbulence intensity is the ratio of the r.m.s. fluctuating longitudinal velocity ( $u'$ , measured with the PWA) at a given location to the mean wind speed at that location. The maximum was observed near  $x=8h$  below  $z=0.5h$ . Intensities of greater than 30% were observed for heights less than  $1.5h$  between  $x=2$  and  $12h$  and at  $x=1h$  just above the windbreak height. A pulsed-wire must be used here because with intensities greater than 25-30% the errors with hot-wire data become large.

The fluctuating velocity component may also be described in absolute terms. Figure 4.4 again shows the distribution of  $u'$ , but normalized by  $U_R(h)$ . The presence of a maximum between  $z \approx 1.25h$  and  $1.5h$  suggests that greater turbulence is generated in the shear layer separating from the top of the windbreak. The turbulence diffuses with downstream distance. The normalized r.m.s. velocity fluctuations were quite low (5-7%) just downstream of the windbreak.

Figure 4.5 shows vertical profiles of the longitudinal mean velocity component (measured with both anemometers) normalized by  $U_R(h)$  as a function of downwind distance. These are compared with the reference wind speed profile. Comparison of the HWA and PWA results show significant differences only in the region of high turbulence intensity. The HWA tended to overestimate the wind speed in the high turbulence region. No flow reversals in the mean occurred, but instantaneous reversals were indicated by the PWA (when the upwind

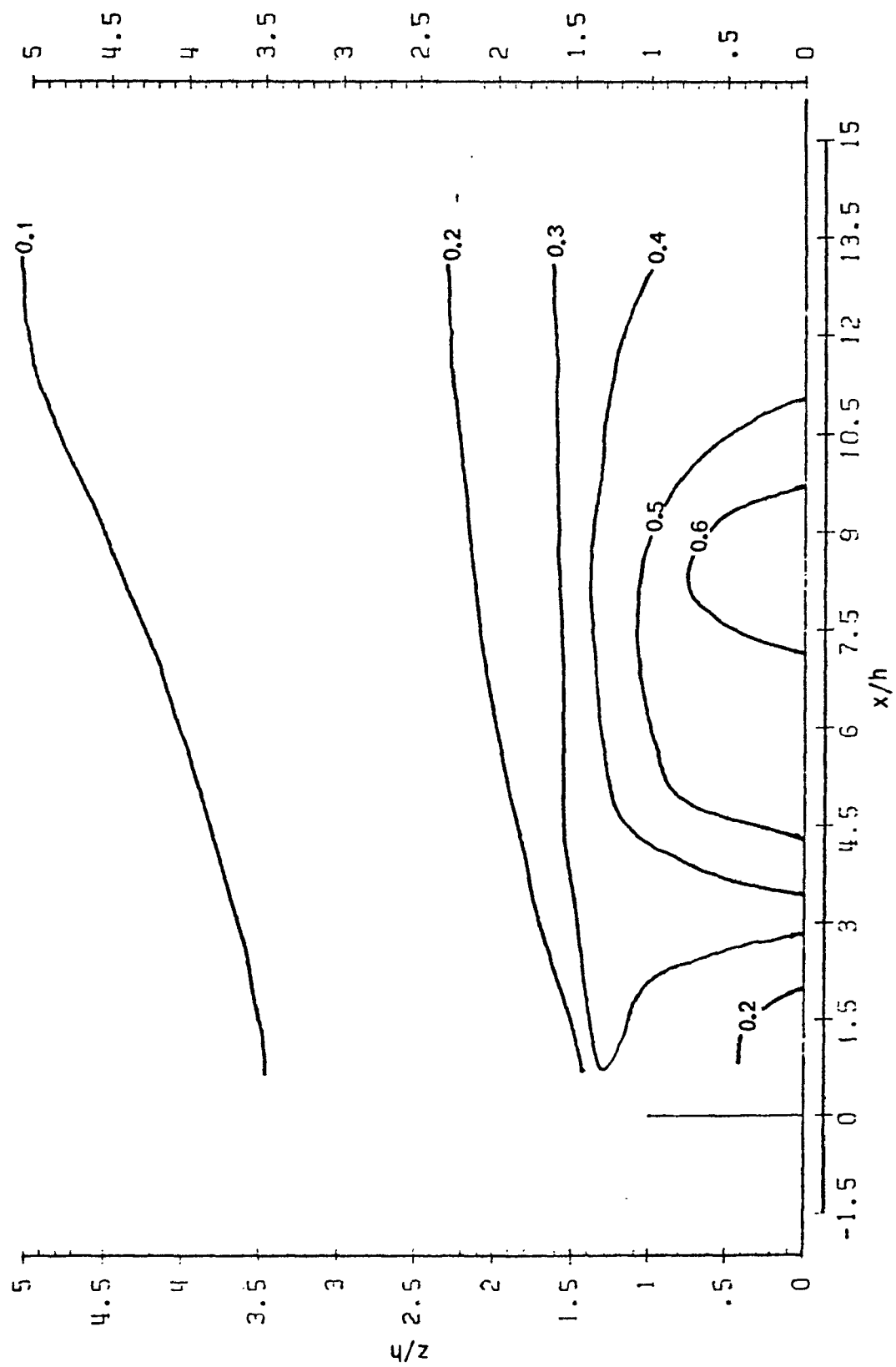


Figure 4.3 Turbulence intensity downstream of a porous windbreak.

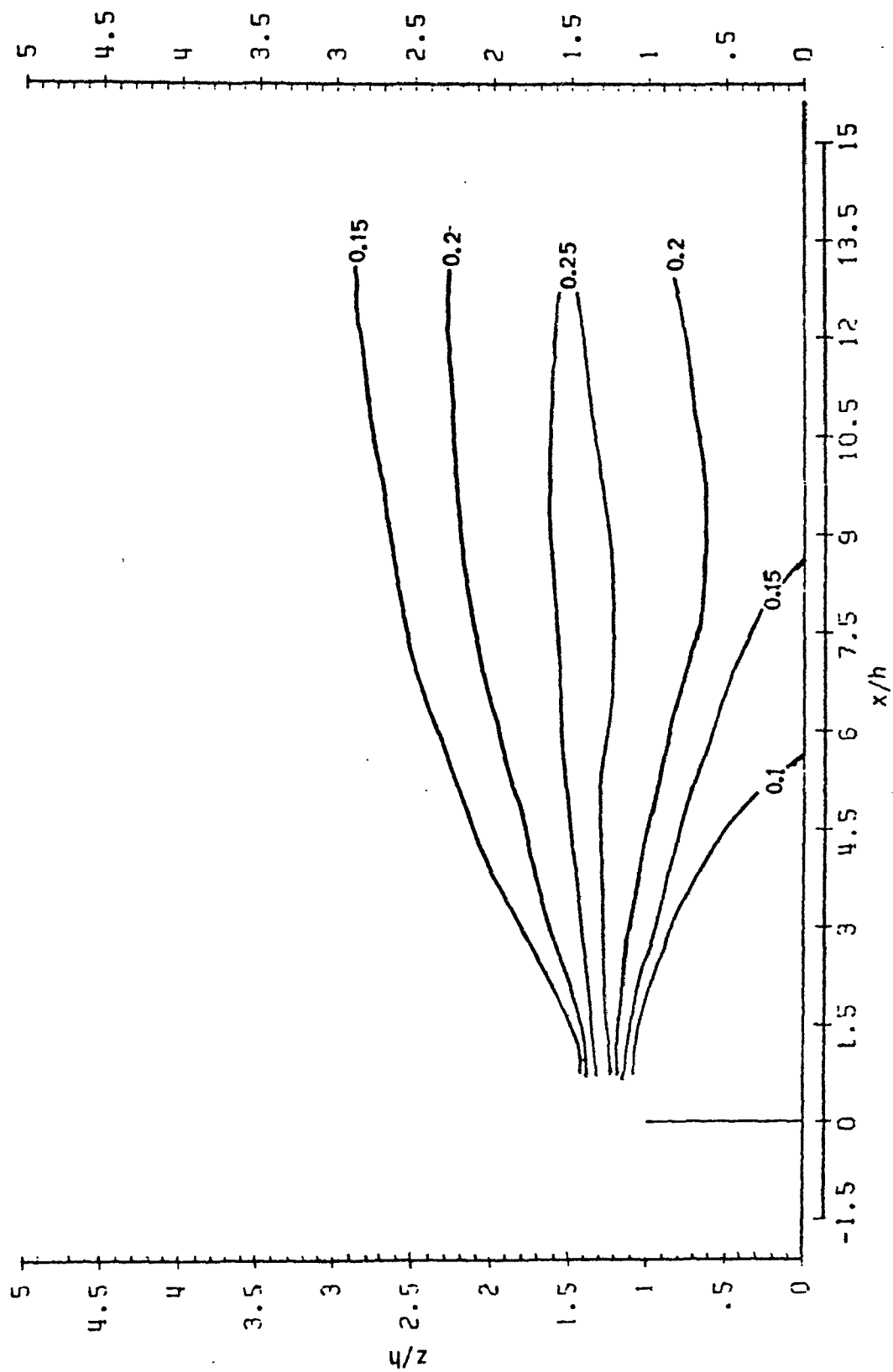


Figure 4.4 Normalized r.m.s. longitudinal velocity fluctuation downstream of a porous windbreak.

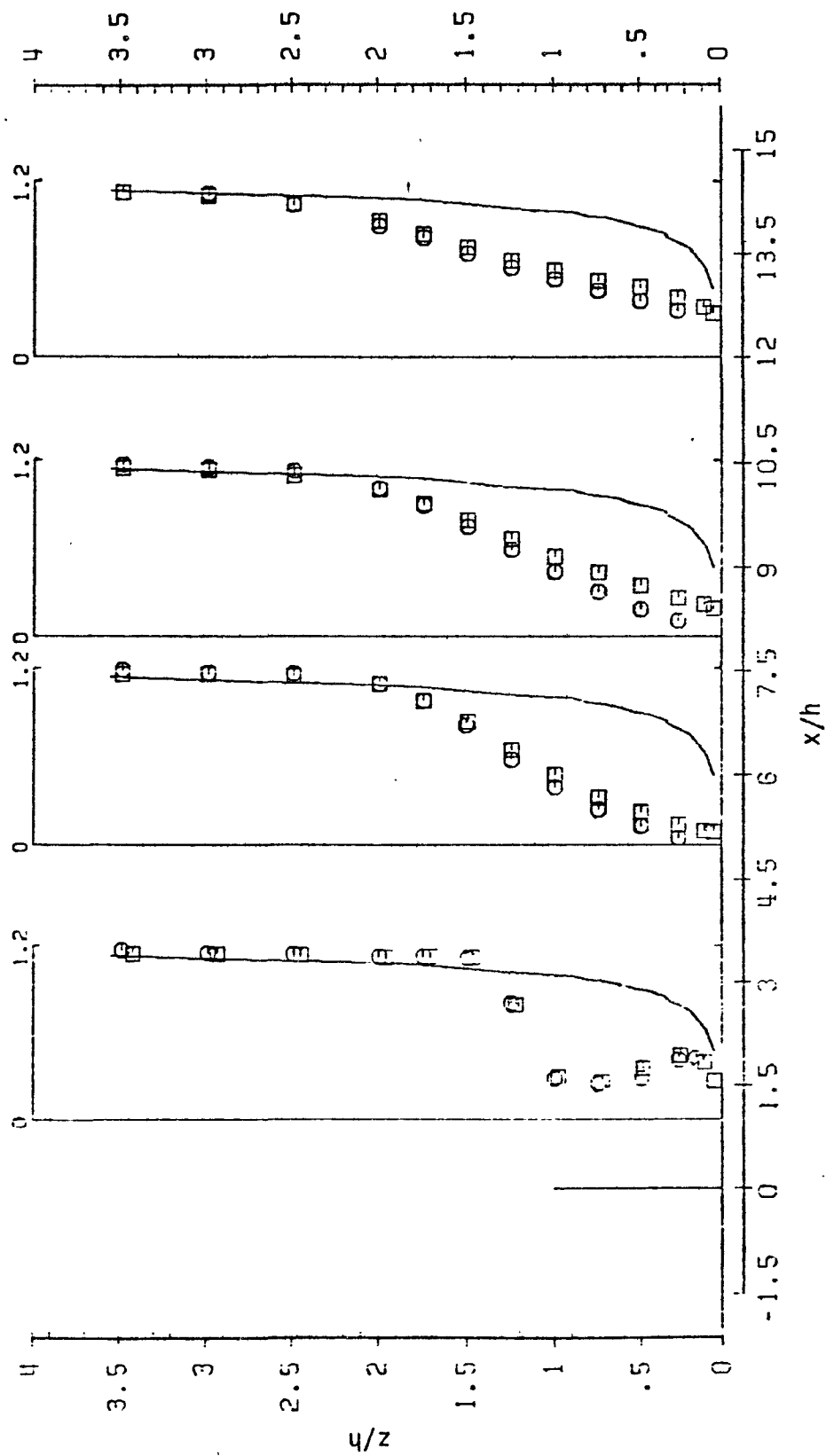


Figure 4.5 Profiles of normalized wind speed downstream of a porous windbreak. Line: reference profile. Circles: pulsed-wire anemometer data. Squares: hot-wire anemometer data.

sensor wire sensed the tracer) and used to calculate the average over the sample time. The HWA time-averaged mean is not a vector average since the flow direction is not sensed. Hence, the PWA wind speeds were smaller than the HWA indicated wind speeds. Again, the profiles show significant reductions in speeds near the surface at  $x=5h$  and  $8h$ . The reductions from the reference values are quite clear.

Figure 4.6 shows vertical profiles of the r.m.s. longitudinal fluctuating velocity component normalized by  $U_R(h)$ . Again, results from the HWA and PWA downstream of the windbreak and the HWA reference profile are shown. The PWA results were shown in Figure 4.4 in a different format. The dashed lines separate the region in which the r.m.s. fluctuations exceed 10% of the reference value from those in which the fluctuations are less than or nearly equal to the reference value. Increased turbulence is quite apparent at  $x=1h$  just above the windbreak height. The maximum fluctuation at each downwind distance is approximately twice the reference value at the same height. The r.m.s. fluctuations in the lower region are approximately half the reference r.m.s. fluctuations at  $x=1h$ . Vertical diffusion of the increased turbulence in the shear layer is again apparent. PWA values tended to be higher than HWA values for heights greater than the windbreak height and slightly less than HWA values for lower heights. The greatest differences were in the region of the highest r.m.s. fluctuations.

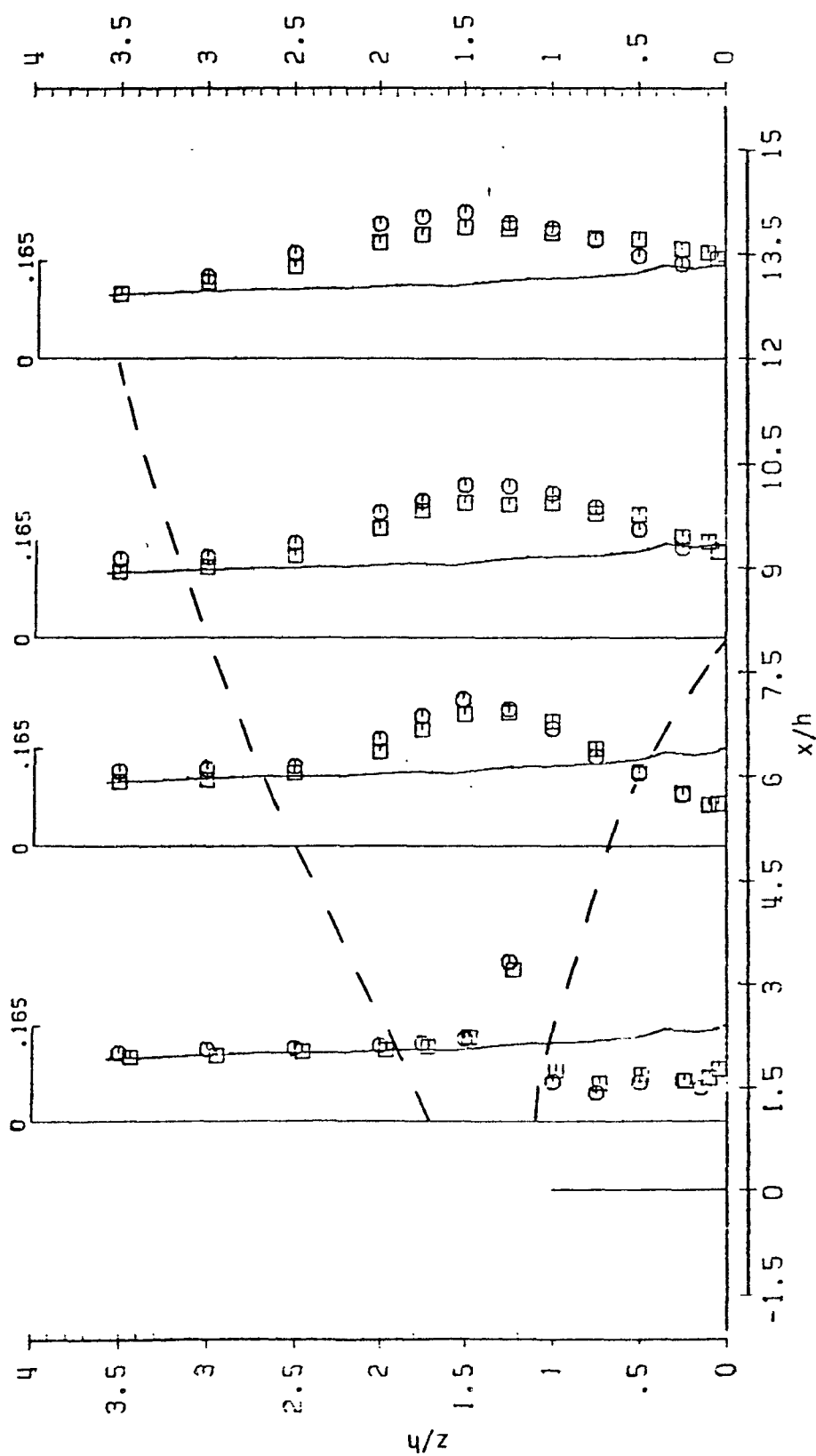


Figure 4.6 Profiles of normalized longitudinal velocity fluctuation downstream of a porous windbreak. Line: reference profile. Circles: pulsed-wire anemometer data. Squares: hot-wire anemometer data. Dashed lines: separate the region in which the fluctuations exceed 10% of the reference value from those in which the fluctuations are less than or nearly equal to the reference value.

## 5. FLOW ABOUT STORAGE PILES

The flow about the two storage piles will be described. It is important to locate the areas of high wind speed since that is where particle uptake is most likely to occur. It is also important to locate the areas of low wind speed; the areas where wind erosion is least likely to occur. The potential fugitive-dust emissions from uncontrolled (no windbreak protection) piles are related to the wind speed distributions shown here.

### 5.1 CONICAL PILE

Figure 5.1 shows the top view of the pile with contours of normalized wind speed,  $u/u_r$ , where  $u$  is the wind speed at the pile surface measured with the thermistor and  $u_r$  is the wind speed at the equivalent full-scale height of 10 m in the absence of the pile. 10 m was chosen as the reference height rather than 11 m, the pile height, because 10 m is the standard height to which "surface" wind speed measurements are usually referenced in the meteorological literature. Note that the air flow in the figure is from the left. The areas of maximum wind speed are near the top of the upwind face but toward the sides of the pile. A high speed region ( $u/u_r > 0.8$ ) is on the upstream face, extending from near the crest down both sides. The area of minimum wind speed is in the lee near the top of the pile with regions of low wind speed extending down the pile on both sides of the centerline. High speeds along the pile sides are expected because the flow is accelerating round the pile. The flow separates on the lee side, resulting in a region of low-speed recirculating flow.

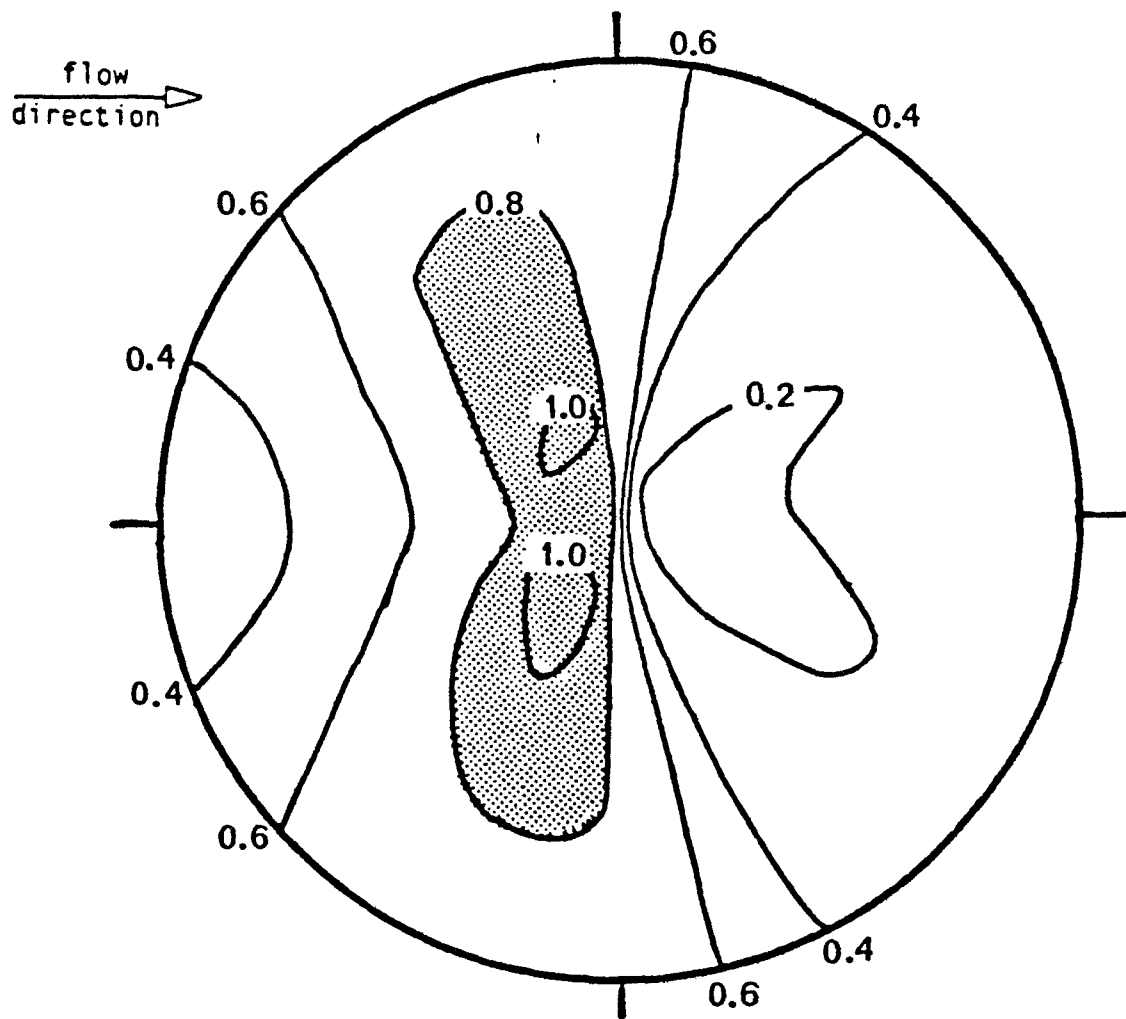


Figure 5.1  $u/u_r$  about conical pile for no windbreak case.

## 5.2 OVAL, FLAT-TOPPED PILE

Flows about the pile oriented with its longer axis normal to the air flow, then at  $20^\circ$  and  $40^\circ$  from the original position are described. Figure 5.2 shows the top view of the pile with contours of normalized wind speed. This was the pile orientation during all the windbreak tests, except for the  $20^\circ$  and  $40^\circ$  pile orientations. The overall pattern, as indicated by the isotachs, is fairly symmetric except for some asymmetry of flow in the lee. Since the thermistors were located in a symmetrical pattern on the pile, a point-to-point comparison of measured wind speed about the axis parallel to the wind direction was made. Several significant differences were observed. Upon completion of the runs with the windbreaks, wind speeds were measured with the pile oriented  $180^\circ$  to its original position. Again, the overall pattern was similar to that shown in Figure 5.2, but point-to-point comparisons about the line of symmetry showed several significant differences. The differences likely resulted, in part, from the sources of error in the thermistor measurements discussed in section 3.2. Further, with nine times as many thermistors on this pile, as compared to the conical pile, errors from applying the calibration equation (Eq. 3.7) to all the thermistors could be greater than that discussed earlier. Considering these uncertainties, the wind speed pattern was corrected based upon the data from the  $0^\circ$  and  $180^\circ$  pile orientations, assuming flow symmetry around the pile surface.

The corrected pattern is seen in Figure 5.3. The highest wind speeds were observed on the windward face near the top of the pile, extending down the sides, similar to the case with the conical pile

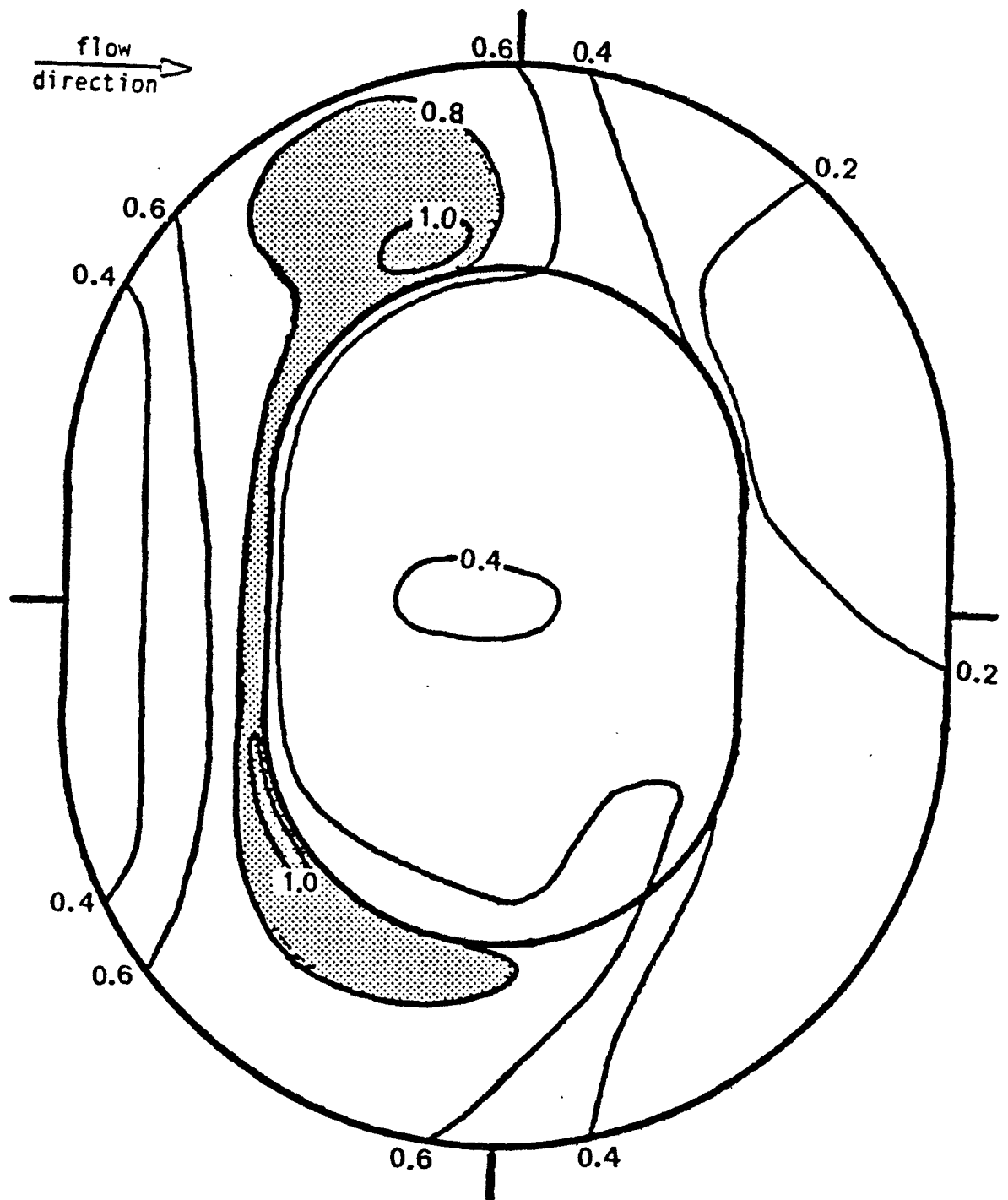


Figure 5.2  $u/u_r$  about oval, flat-topped pile for no windbreak case.

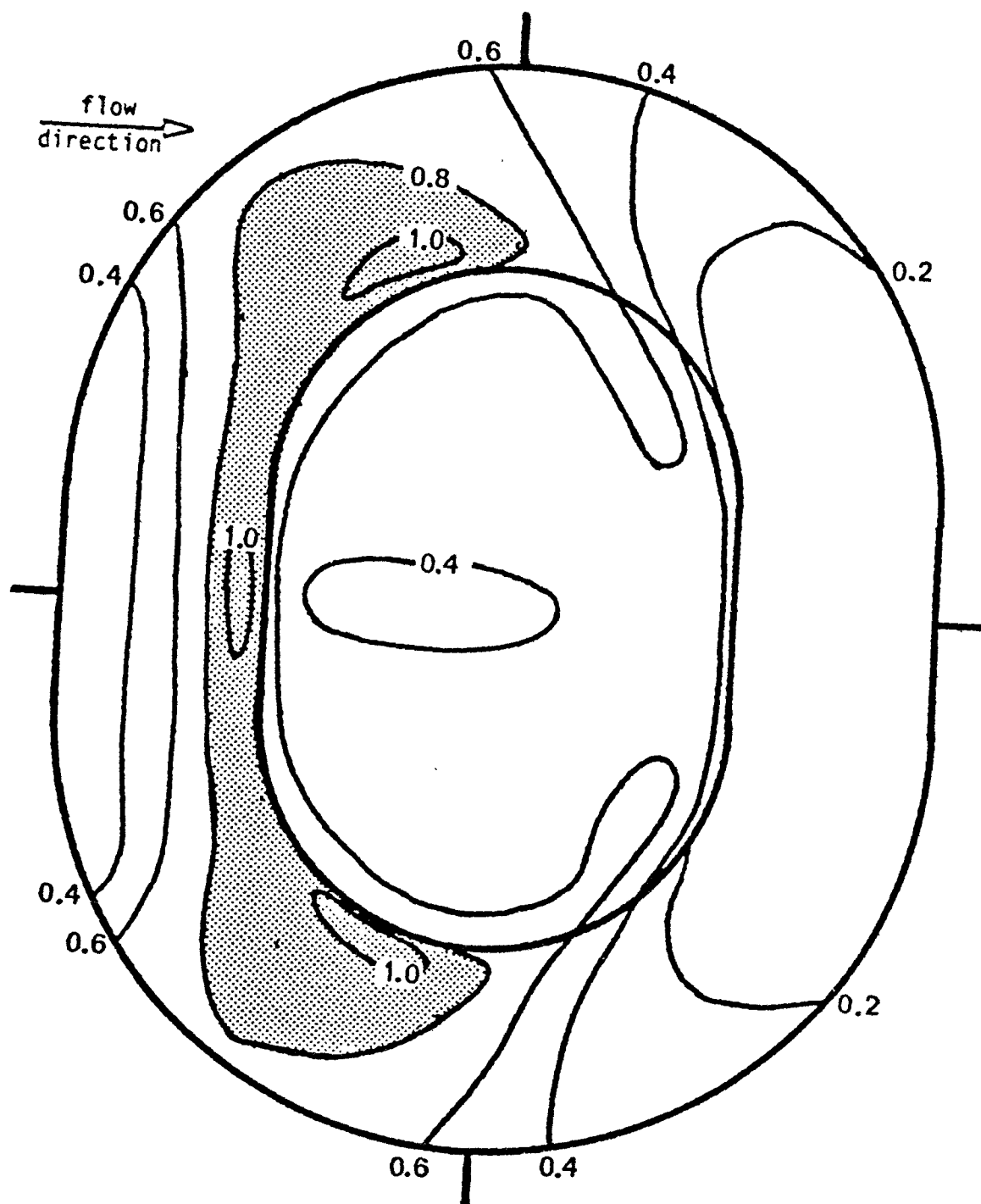


Figure 5.3 Corrected  $u/u_r$  about oval, flat-topped pile for no windbreak case.

Again, the lowest speeds were observed in the lee; but a secondary minimum also occurred on the top of the pile.

Thermistor derived wind speed values for the cases with a windbreak were also corrected. The correction factor for each thermistor was the percentage difference between the value measured with the pile in the  $0^\circ$  position and the corrected value, both in the absence of any windbreak. The data for all the windbreak cases and for all the pile orientations were corrected, using the same correction factors which ranged in magnitude from 0% to 50%, with 82% of the correction factors being within  $\pm 20\%$ .

The normalized wind speed patterns for the pile oriented at  $20^\circ$  and  $40^\circ$  from its original position normal to the air flow are shown in Figure 5.4. The band of high speed near the top of the upstream face was observed for both orientations. The lobes of high speed extending toward the base on the sides shifted with pile orientation.

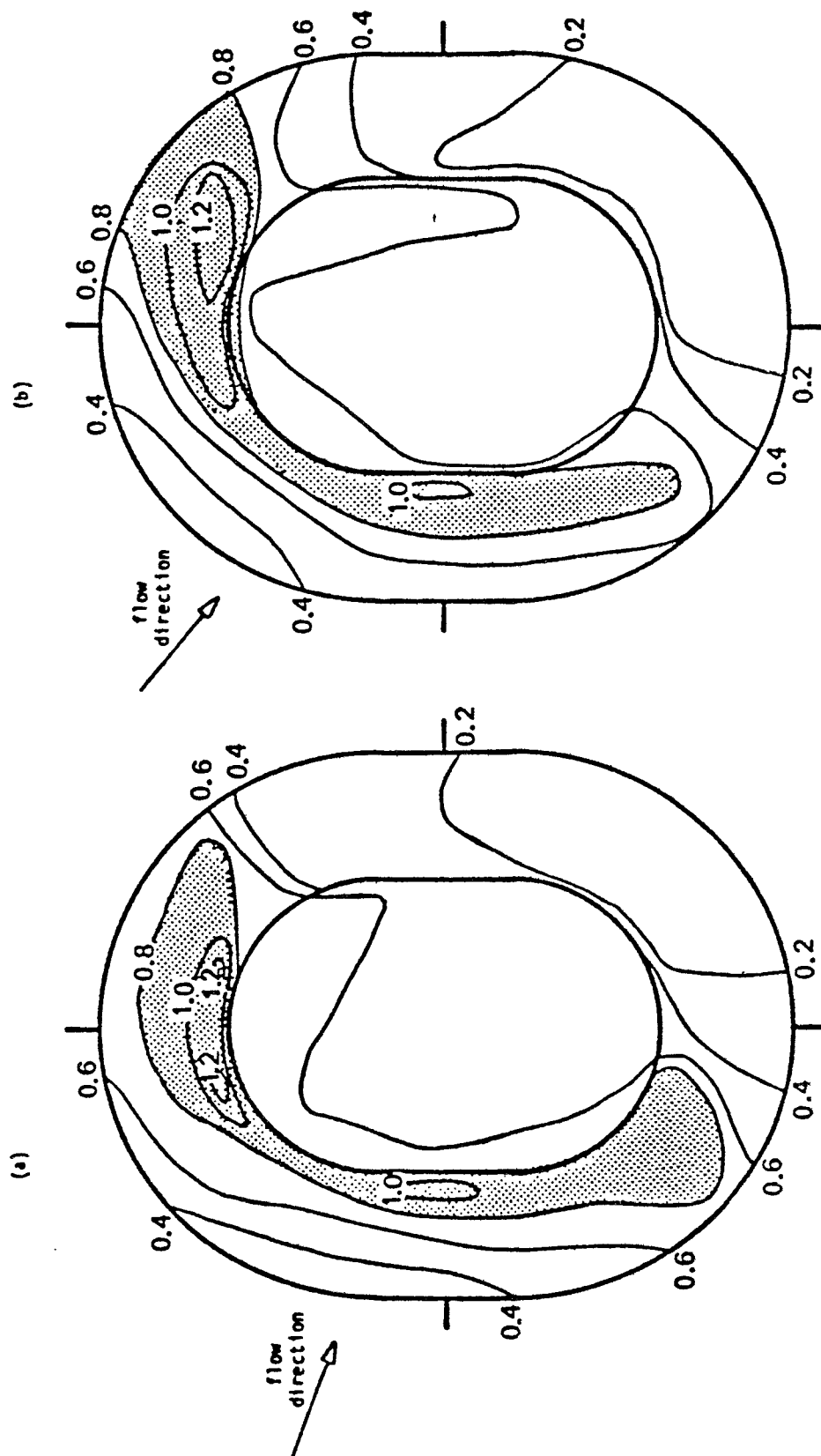


Figure 5.4 Corrected  $u/u_r$  about oval, flat-topped pile at an angle to incident flow for no windbreak case: (a) 20°, (b) 40°.

## 6. WINDBREAK EFFECTS ON FLOW ABOUT STORAGE PILES

The use of windbreaks for storage-pile fugitive-dust control is based upon the existence of a sheltered region downstream of a windbreak. Effects of windbreak height, length, porosity and position on wind speed about the piles are discussed for the case of a windbreak placed upstream of the piles and on the top of the flat-topped pile. Relative wind speed reduction and the observed maximum wind speed are used to assess the relative effectiveness of the various windbreaks.

### 6.1 WINDBREAK UPSTREAM OF THE PILE

Before the results are presented, general windbreak effects are hypothesized based upon flow structure and pile location in the sheltered region.

#### 6.1.1 Relation to flow structure

Since height and width of the sheltered region are directly related to windbreak height and length, windbreaks placed upstream of the pile having dimensions less than the pile height or length are expected to be less efficient as are smaller windbreaks placed on the pile top. Wind speed reductions downstream of a windbreak were greatest near the surface and decreased with height (Figure 4.2). Although some reductions were observed at heights greater than the windbreak height, little, if any, reductions were observed at  $z=2h$ . Therefore, windbreaks of height  $\leq 0.5H$  cannot be expected to have much effect on reducing the high wind speeds occurring near the tops of the piles; the effect may be greater when the pile is farther from the windbreak since the height of the sheltered region increases with downwind distance. Similarly, windbreaks of length less than the pile base length are expected to be

less effective since the pile is not "fully within" the sheltered region.

Figures 6.1 and 6.2 show a superposition of the conical and oval, flat-topped piles' cross-sections at the 1H and 3H positions for the three windbreak heights onto the "streamlines" downstream of a windbreak of length 10.5 times its height (Figure 4.1). Streamlines in the pile's presence are not the same as those shown; the location of the low wind speed region with respect to the pile is of interest here. The upstream face of both piles is in the same relative position, but the difference in pile size is quite apparent. For the 0.5H high windbreak, the upstream face is in a lower wind speed area when the pile is in the 1H rather than the 3H position. For the 1.0H and 1.5H high windbreaks, however, the upstream pile face is in a lower wind speed region when the pile is in the 3H position. The pile may be in an even lower wind speed region at 6H for the 1.5H high windbreak.

#### 6.1.2 Results

Windbreak effects on surface wind speed patterns are discussed in this subsection. Windbreaks were placed upstream of both piles, normal to the wind direction, and at an angle to the wind direction with the conical pile. The cases with a windbreak normal to the air flow are discussed first. Figures showing normalized wind speed for many of the windbreak cases are not included because the change in wind speed due to a windbreak is of more interest. With a windbreak, the wind speed at a given location on the pile surface is some fraction of that in the unprotected case. The relative amount by which the wind speed is reduced is called the wind speed reduction factor  $R_i$  and, in percent,

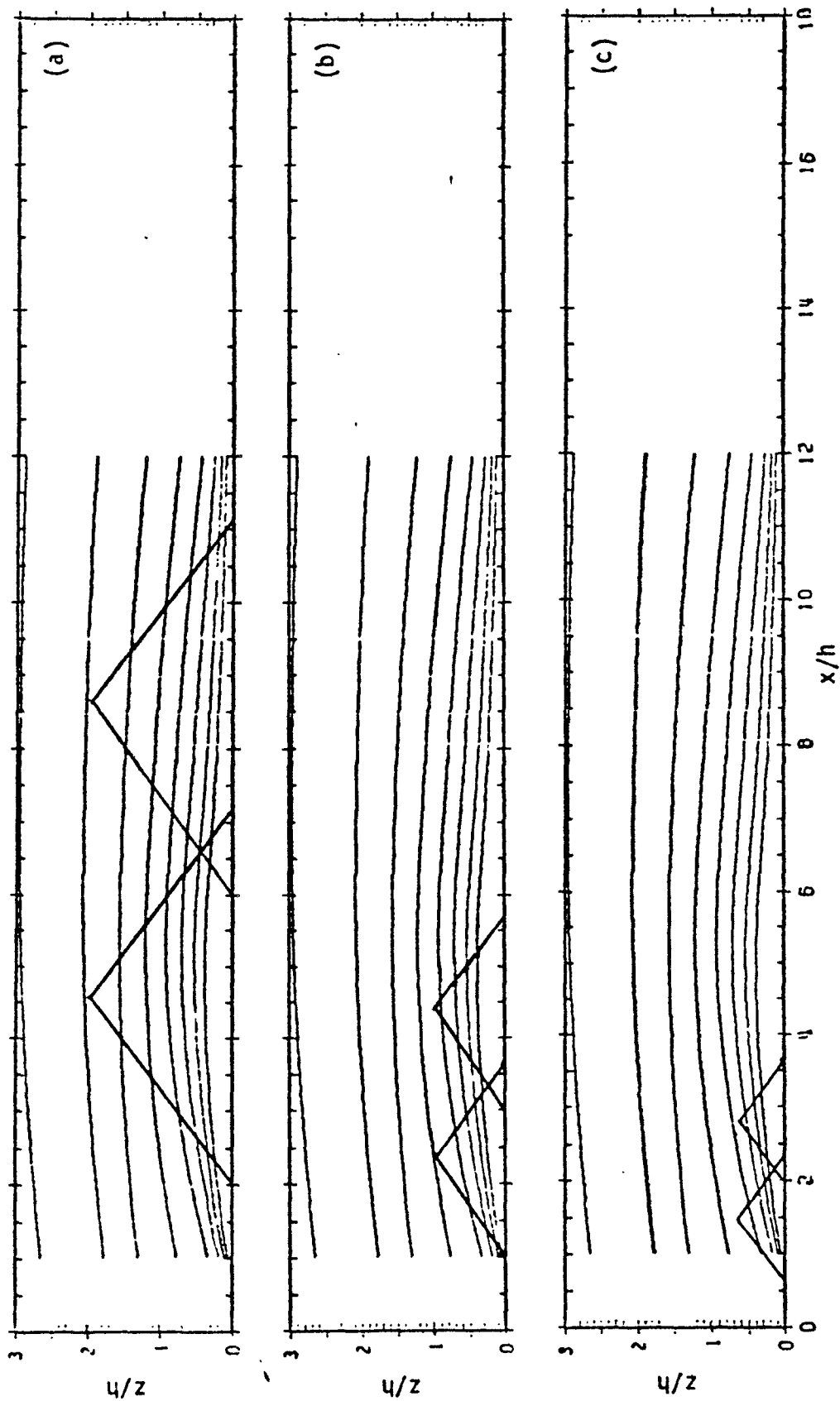


Figure 6.1 Superposition of conical pile positions and undisturbed "streamlines" downstream of a porous windbreak of height: (a) 0.5H, (b) 1.0H, (c) 1.5H.

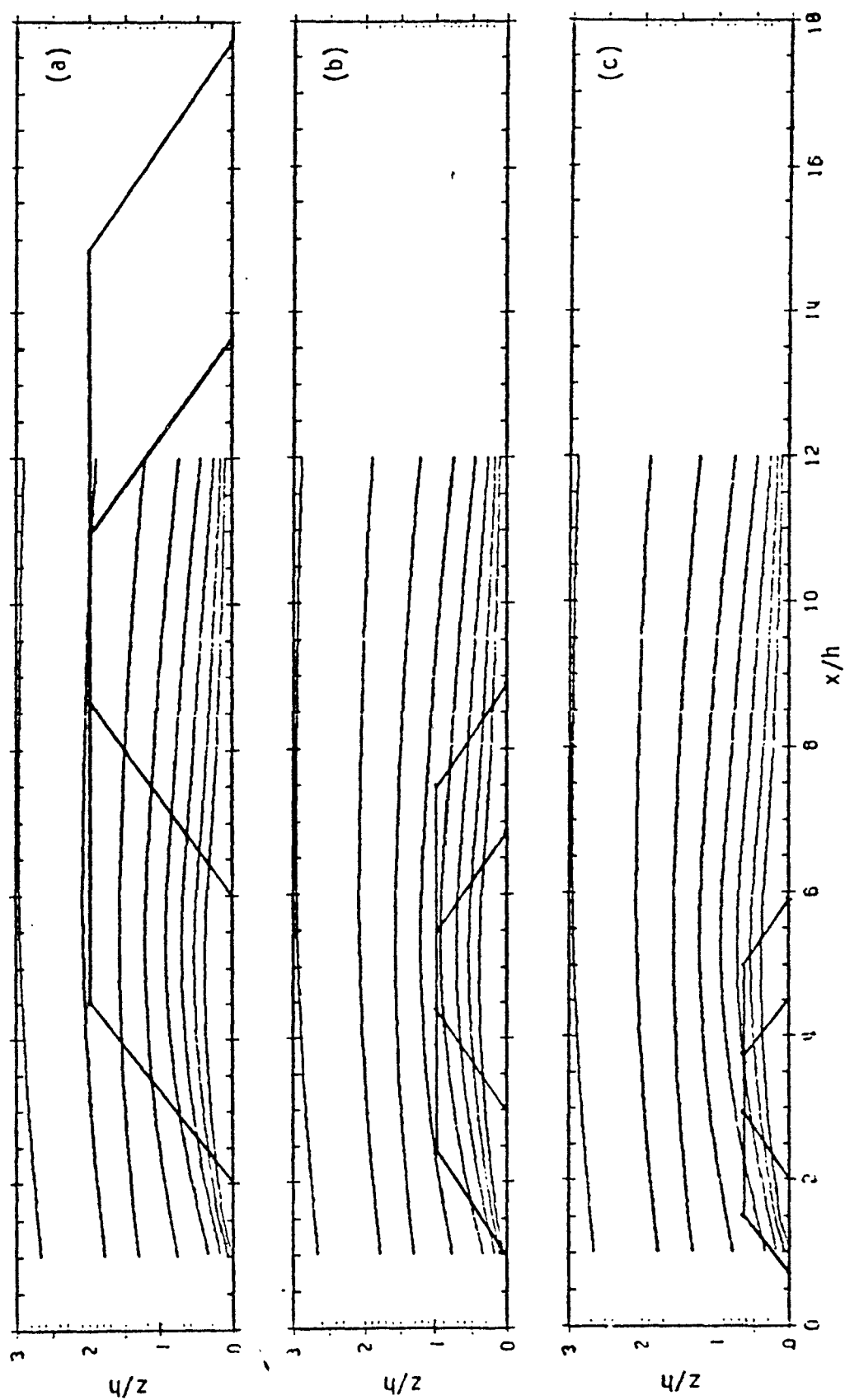


Figure 6.2 Superposition of oval, flat-topped pile positions and undisturbed "streamlines" downstream of a porous windbreak of height: (a)  $0.5H$ , (b)  $1.0H$ , (c)  $1.5H$ .

is defined as

$$R_i = (u_{0,i} - u_i)/u_{0,i} \times 100, \quad (6.1)$$

where  $u_i$  and  $u_{0,i}$  are wind speeds at the  $i$ -th location on the pile for the cases with and without the windbreak, respectively.  $R_i$  is zero when the windbreak causes no change in the wind speed, and 100% when the wind speed is reduced to zero.  $R_i$  of 25% means that the wind speed resulting from the windbreak's presence is 25% less than the wind speed in the unprotected case. It is important to remember that the combined effects of windbreak height, length, porosity, and position, as well as turbulence in the approach flow, and pile shape and surface roughness determine the wind speed distribution over the pile surface. Some of these factors will be considered here.

An optimum windbreak size (height and length) exists since a very small windbreak is expected to be ineffective and a very large windbreak may be effective in reducing wind speeds but may turn out to be too expensive. Contours of constant wind speed reduction factor  $R_i$  resulting from the 65% porous screen of height  $0.5H$ , located  $1H$  from the pile base and length  $1.0D$  (Figure 6.3) and  $1.0B$  (Figure 6.4) are shown. Referring also to Figures 5.1 and 5.2, in the areas of maximum wind speed of the no windbreak cases, these windbreaks reduced the wind speed by approximately 20%. For both piles, relatively large reductions were observed over approximately the lower three-fourths of the upstream face, with the greatest reductions apparent near the piles' centerlines. Regions of wind speed increase (negative reduction factor) were observed on the lee side of the conical pile and on the top, upstream half of the larger pile. The increase in speed observed on the top of the

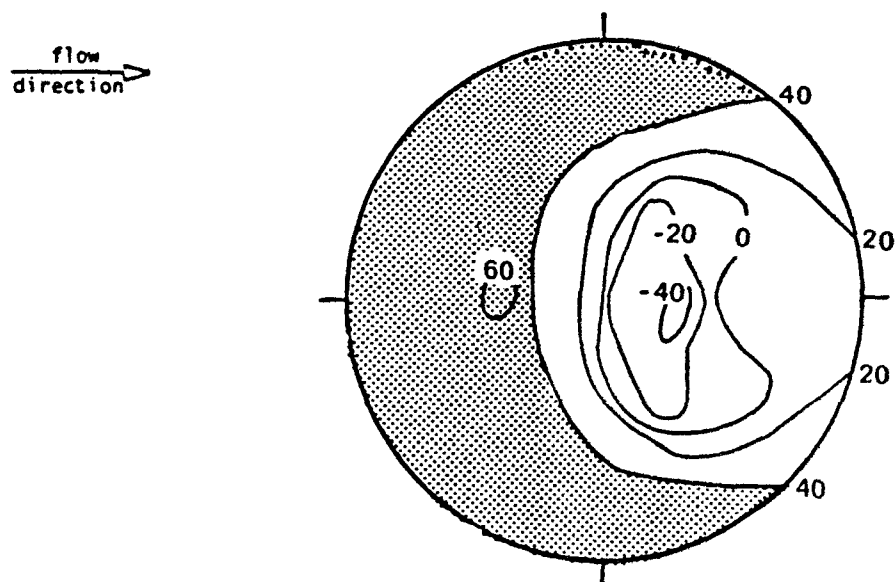


Figure 6.3 Wind speed reduction factor for the 65% porous windbreak of height  $0.5H$  and length  $1.0D$  placed  $1H$  from the conical pile base.

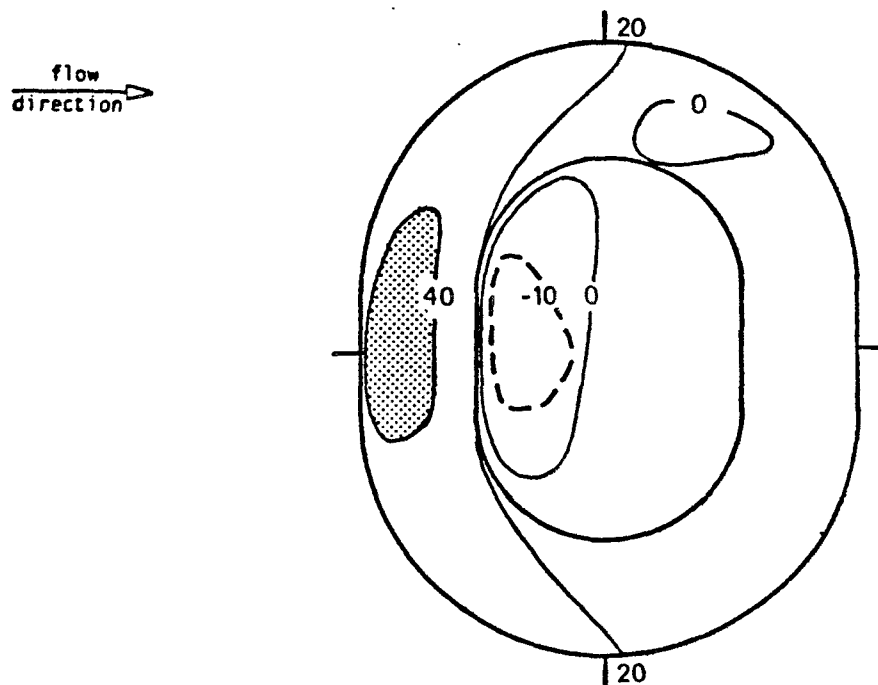


Figure 6.4 Wind speed reduction factor for the 65% porous windbreak of height  $0.5H$  and length  $1.0B$  placed  $1H$  from the oval, flat-topped pile base.

larger pile may be due to a combination of air deflection about the windbreak and the pile. In terms of fugitive dust control, these increases are probably not significant for the conical pile because the wind speeds will be relatively low in this region unless the reference speed ( $u_r$ ) is very high, but the increase could be significant for the larger pile, again depending on  $u_r$ . This general pattern of high wind speed reduction in the lower portion of the upstream face and increase in the conical pile upper lee region and the top upstream half of the oval, flat-topped pile was typical of all the windbreaks of height  $0.5H$ , but not of the higher windbreaks.

Slight asymmetry is apparent in the lee of the larger pile in Figure 6.4; this was also observed in the presence of other windbreaks. Since the wind speeds are low in the lee, even a small change in wind speed appears as a large relative change in the reduction factor.

For higher windbreaks (heights  $1.0H$  and  $1.5H$ ) upstream of the conical pile, the area of greatest wind speed reduction was the upper part of the windward side, with typical reductions of at least 50%. Areas of negative reduction factors (up to  $\approx -15\%$ ) were observed with windbreaks of height  $1.0H$  located  $3H$  from the conical pile; these areas were significantly smaller than those observed with lower windbreaks (Figure 6.3). Wind speeds were reduced everywhere for the other higher windbreaks with reduction factors ranging from 15% to 60% on the lee side. The reduction pattern for windbreaks of the same porosity, length, and position did not differ significantly when the windbreak height was increased from  $1.0H$  to  $1.5H$ , except for the least porous windbreak located farther ( $3H$ ) from the pile. In that case, the

highest windbreak caused the greatest reductions over much of the pile. The reductions in the lee near the pile top also were higher for the 1.5H high windbreak.

For higher windbreaks (heights 1.0H and 1.5H) upstream of the oval, flat-topped pile, wind speeds were reduced everywhere. Increasing the height from 1.0H to 1.5H gave greater reductions on the pile top, but the general pattern of wind speed reduction depended upon the windbreak location. In general, a windbreak of height 1.0H located 1H upwind of the pile base gave similar wind speed reductions ( $R_i$ ) on the top part of the upstream face and on the pile top. Increasing the height to 1.5H caused greater reductions only on the pile top. A windbreak of height 1.0H in the 3H position caused higher reductions on the upstream face than on the pile top. Increasing the height increased the reductions on the top to approximately the same values as those on the upstream face. Relative reductions of 30% to 60% occurred over most of the top part of the upstream sloping face when windbreaks of heights 1.0H and 1.5H were close to the pile (the 1H position); for windbreaks of both heights at the 3H position, the corresponding range of reduction factors was 45% to 75%. The increase in wind speed reduction on the top of the pile with windbreak height increasing from 1.0H to 1.5H was greater for windbreaks located 3H from the pile base (e.g., for 50% porous windbreaks at the closer position, the reduction increased from approximately 50% to 70%, but at the farther position, it increased from approximately 30% to 60%).

To summarize, windbreak height is clearly important, as hypothesized in section 6.1.1. The 0.5H high windbreak is not as

effective as higher windbreaks ( $1.0H$  and  $1.5H$ ), because the former reduces wind speeds over a smaller portion of the pile. Higher windbreaks reduce wind speeds over a larger part of the pile's surface and cause greater reductions in the regions of high wind speed observed in the no windbreak case. In general, with increasing windbreak height the wind speed reductions increase also and cover a greater portion of the pile, but with a conical pile, the windbreak as high as the pile is nearly as effective as a higher one.

Increasing length is expected to effect greater reductions at the pile sides. This was observed with the 50% porous windbreaks, although the difference was slight as the length was increased from  $1.0D$  to  $1.5D$  and from  $1.0B$  to  $1.5B$  with the conical and larger piles, respectively. Windbreaks of length less than the pile base were also placed upstream of the oval, flat-topped pile. The length was equal to the maximum length of the pile at the top. Very high speeds were observed on the upstream sloping face near the pile sides with these windbreaks. Longer windbreaks located upwind of the pile base caused much higher reductions in wind speeds along the sloping sides and slightly higher reductions at the sides of the flat pile top. The reduction factors for the two 50% porous windbreaks of height  $1.5H$  at the  $1H$  position are shown in Figure 6.5. The effect of length at the sides is quite evident. Length becomes even more important if the incident wind is not normal to the windbreak (see later discussion in this subsection).

Porosity was another windbreak parameter under investigation. For a given windbreak height, length, and position, greater wind speed reductions occurred for the less porous (50%) windbreak, particularly on

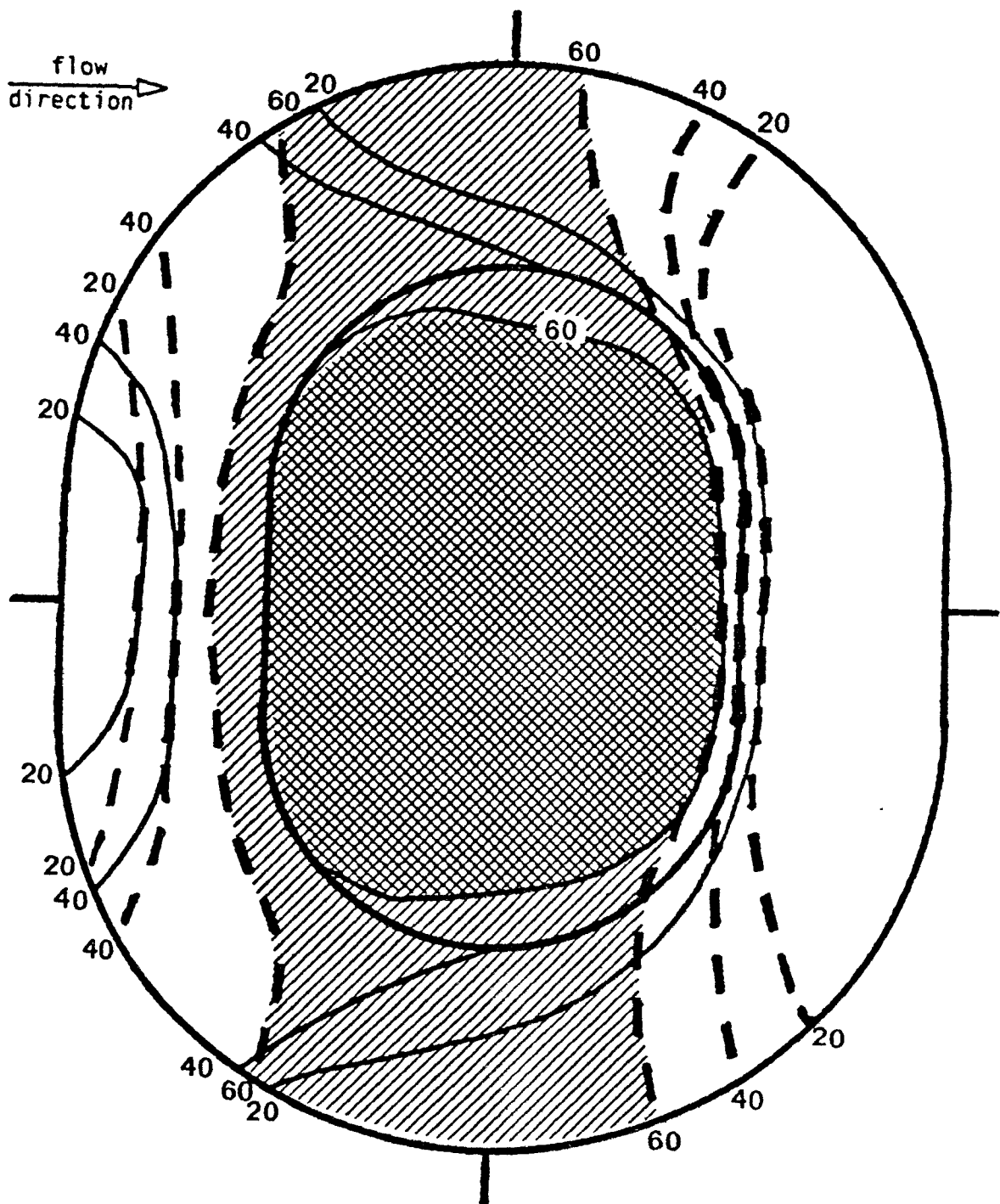


Figure 6.5 Wind speed reduction factor for the 50% porous windbreak of height  $1.5H$  placed  $1H$  from the oval, flat-topped pile base with length  $0.6B$  (solid line) and  $1.0B$  (dashed line).

the windward face and top of the piles. The reduction factors for the two different porosity windbreaks of height  $1.0H$  and length  $1.0D$  located  $1H$  from the conical pile and the two windbreaks of height  $1.0H$  and length  $0.6B$  located  $1H$  from the oval, flat-topped pile are shown in Figures 6.6 and 6.7, respectively. In both cases the distributions are quite similar in shape, with larger reductions in the 50% porous case.

The last windbreak parameter studied was the distance between the windbreak and pile. As discussed earlier, the effect of windbreak position appears to be related to windbreak height. Windbreaks of height  $0.5H$  caused greater wind speed reduction in the lower part of the windward face and towards the sides when placed  $1H$ , rather than  $3H$ , from the piles' bases, although slightly higher reductions were observed along the top of the slope of the oval, flat-topped pile when the  $0.5H$  high windbreak was at the  $3H$  position. Windbreaks of height  $1.0H$  placed  $3H$  from either pile caused greater wind speed reduction on the windward face, but for the conical pile, less reduction in the lee. Windbreaks of height  $1.5H$  placed  $3H$  from either pile caused greater wind speed reductions on the windward face than if the windbreak were at the  $1H$  position. However, for windbreaks of height  $1.0H$  and  $1.5H$  with the oval, flat-topped pile, the reduction on the pile top was less when the windbreak was in the  $3H$  position. For both piles, the reductions near the centerline along the pile slope were low near the pile base and high towards the top of the slope with windbreaks greater than  $0.5H$  high at the  $1H$  position. In the  $3H$  position, slightly higher reductions occurred near the top of the piles on the windward face and much higher reductions occurred in the lower portion such that the

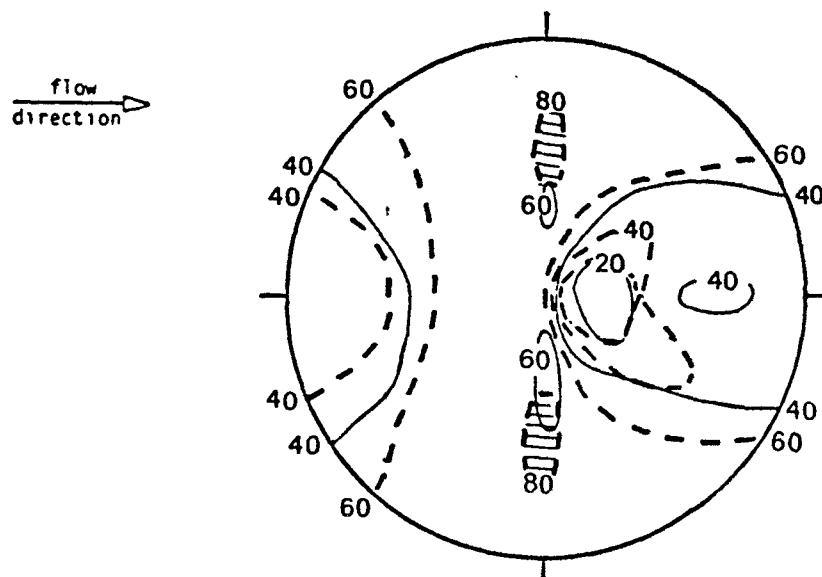


Figure 6.6 Wind speed reduction factor for the windbreak of height  $1.0H$  and length  $1.0D$  placed  $1H$  from the conical pile base with porosity 65% (solid line) and 50% (dashed line).

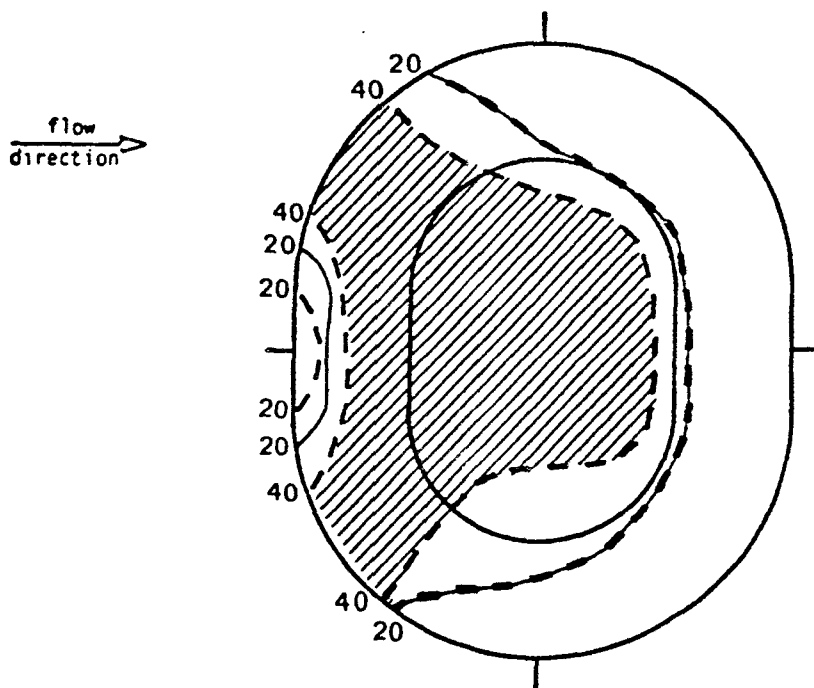


Figure 6.7 Wind speed reduction factor for the windbreak of height  $1.0H$  and length  $0.6B$  placed  $1H$  from the oval, flat-topped pile base with porosity 65% (solid line) and 50% (dashed line).

reductions tended to be uniform along the slope. Figures 6.8 and 6.9 show the wind speed reduction distributions for the two windbreak locations (1H and 3H) for the 1.5H, high 50% porous windbreaks of length 1.5D placed upstream of the conical pile, and length 0.6B placed upstream of the larger pile. Clearly, larger areas of high reduction occurred for the 3H location with the conical pile. Higher reductions occurred over much of the upstream face of the larger pile whereas lower reductions occurred on the top for the 3H case. Hence, the overall effect would depend upon the relative magnitudes of the local effects.

Patterns of wind speed reduction factors clearly show effects of windbreak height, length, porosity and position. The maximum wind speed, independent of position, may also be used to assess relative effectiveness of the various windbreaks since it is related to the maximum particle emission rate. Values of maximum wind speed normalized by the wind speed at the equivalent full-scale height of 10 m in the absence of the pile ( $u_r$ ) for the windbreak cases are given in Tables 6.1 and 6.2 for the conical and oval, flat-topped piles, respectively. Note that the ratio  $u_{\max}/u_r$  is 1.16 and 1.12 for the unprotected (no windbreak) cases. In general, higher maximum wind speeds were observed for windbreaks upstream of the oval, flat-topped pile than for the corresponding windbreak with the conical pile, although many trends were the same for both piles.

All the windbreaks reduced maximum wind speed, which is desired for fugitive dust control. Windbreaks of height 0.5H caused much higher  $u_{\max}/u_r$  than did the higher windbreaks. Differences in  $u_{\max}/u_r$

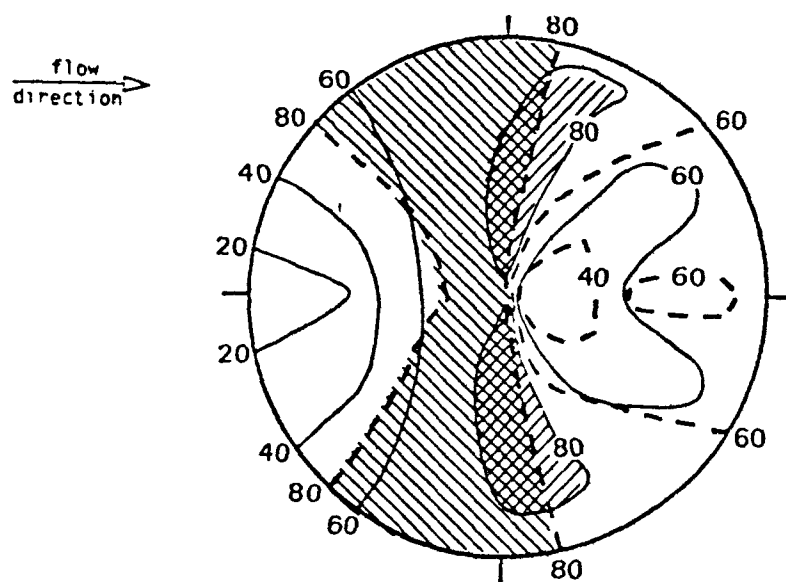


Figure 6.8 Wind speed reduction factor for the 50% porous windbreak of height  $1.5H$  and length  $1.5D$  placed  $1H$  (solid line) and  $3H$  (dashed line) from the conical pile base.

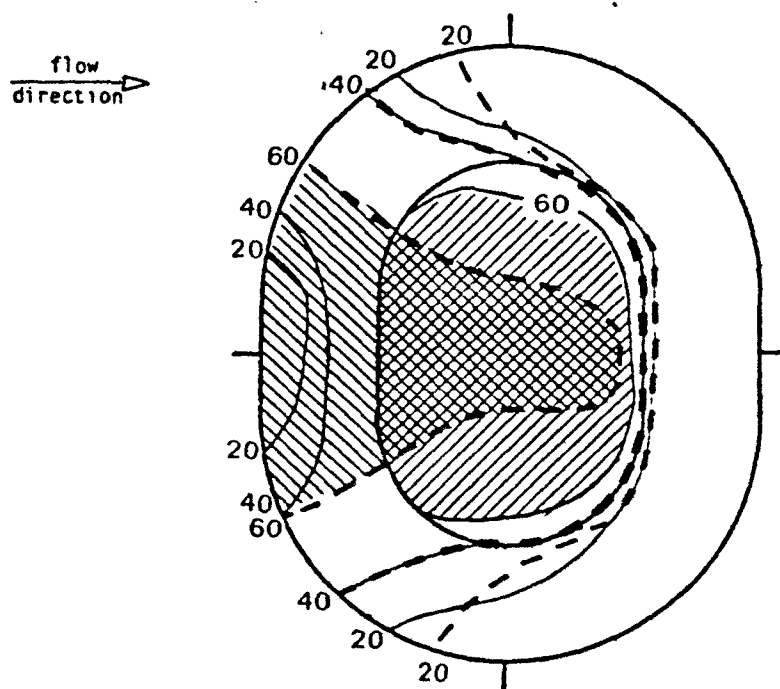


Figure 6.9 Wind speed reduction factor for the 50% porous windbreak of height  $1.5H$  and length  $0.6B$  placed  $1H$  (solid line) and  $3H$  (dashed line) from the oval, flat-topped pile base.

TABLE 6.1  $u_{\max}/u_r$  FOR THE VARIOUS WINDBREAKS PLACED UPSTREAM OF THE CONICAL PILE

65% porous windbreak					50% porous windbreak			
position:	1H		3H		1H		3H	
length:	1.0D	1.5D	1.0D	1.5D	1.0D	1.5D	1.0D	1.5D
height								
0.5H	0.91	0.93	0.91	0.94	0.90	0.93	0.82	0.86
1.0H	0.55	0.59	0.54	0.56	0.31	0.34	0.37	0.27
1.5H	0.56	0.60	0.50	0.52	0.39	0.42	0.25	0.17

TABLE 6.2  $u_{\max}/u_r$  FOR THE VARIOUS WINDBREAKS PLACED UPSTREAM OF THE OVAL, FLAT-TOPPED PILE

65% porous windbreak					50% porous windbreak				
position:	1H		3H		1H			3H	
length:	0.6B	1.0B	0.6B	1.0B	0.6B	1.0B	1.5B	0.6B	1.0B
height									
0.5 H	0.98	0.96	0.97	----	0.95	0.92	0.90	0.93	0.87
0.75H	----	----	----	----	----	0.58	----	----	0.66
1.0 H	0.85	0.70	0.84	0.68	0.73	0.45	0.52	0.78	0.56
1.25H	----	----	----	----	----	0.48	----	----	0.36
1.5 H	0.78	0.69	0.79	----	0.63	0.45	0.49	0.66	0.28

between windbreaks of height 1.0H and 1.5H, for the same porosity, length, and position, were not nearly as great as for those between 0.5H and 1.0H. In general, for a given windbreak height, length, and position, the 50% porous windbreak caused lower  $u_{\max}/u_r$  than did the 65% porous windbreak. Placing a given windbreak a distance 3H from the pile base was more effective than placing it 1H from the conical pile for nearly all the cases tested here. For the larger pile, the 1H position tended to be more effective except for the higher, longer 50% porous windbreaks and differences in  $u_{\max}/u_r$  between the two positions for the 65% porous windbreak were not significant. Windbreaks shorter than the length of the pile base were clearly less effective.

Given a windbreak height, length, porosity and location, the direction of the incident wind will also affect the wind speed reductions about a pile. Wind direction effect was studied with the 50% porous windbreak of height 1.0H, length 1.0D, placed 1H from the conical pile base. Since the wind direction is constant in a wind tunnel, a windbreak oriented at an angle to the tunnel centerline simulates a full-scale case of a fixed windbreak with the air flow at an angle to the windbreak different from normal. Figure 6.10 shows reduction factors for wind directions normal to the windbreak, and at 20°, and 40° to the normal. The windbreak positions are also shown in the figures. The maximum  $u/u_r$  was 0.31, 0.69, and 1.12 for the 0°, 20°, and 40° cases, respectively. For the 20° case, a region of much lower reductions was observed on the side of the pile opposite the windbreak, indicating that the windbreak length and position are important. For the 40° case, the region of reductions greater than 40%

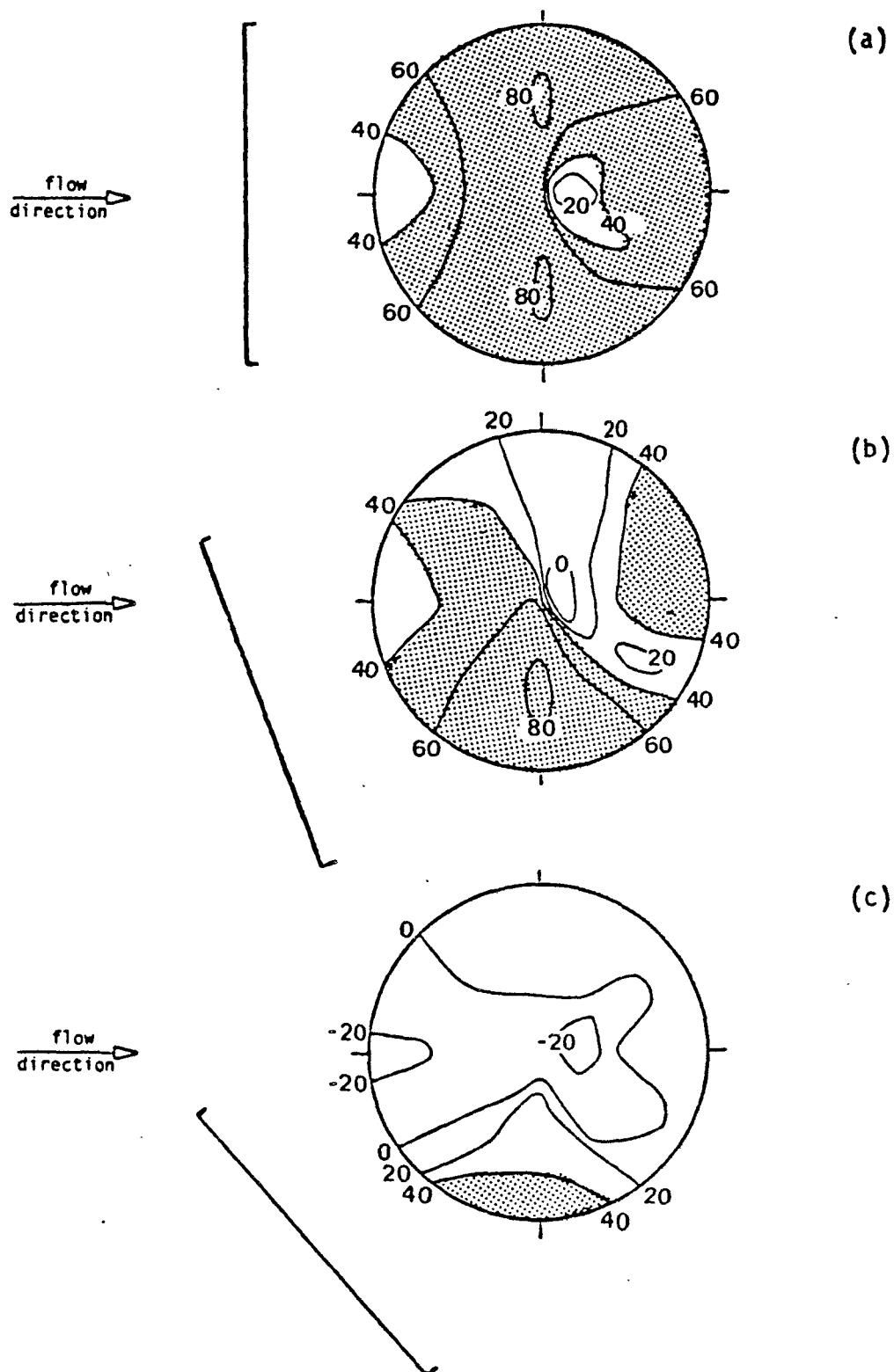


Figure 6.10 Wind speed reduction factor for the 50% porous windbreak of height  $1.0H$  and length  $1.0D$  placed  $1H$  from the conical pile base oriented (a) normal, (b)  $20^\circ$ , and (c)  $40^\circ$  to the flow direction.

was quite small; indeed wind speed increases were observed. Clearly, windbreak effectiveness decreases with increasing angle of flow from the normal.

## 6.2 WINDBREAKS ON THE PILE TOP

In addition to placing windbreaks upstream of both piles, they were placed on the top of the oval, flat-topped pile in the positions shown in Figure 6.11. As stated earlier, the 65% porous windbreaks were of two heights and two lengths and were placed either near the leading edge or centerline of the pile. For a given windbreak in both positions, the pile was rotated  $20^\circ$  and  $40^\circ$  from the original position to assess wind direction effects.

Large reduction factors (up to 65%) on the pile top were observed for all the cases. The location and extent of the area with significant wind speed reduction depended upon windbreak size, location, and angle of the incident flow. Higher, longer windbreaks caused larger sheltered regions as shown in Figure 6.12. The width of the sheltered region (parallel to the windbreak) is larger than the windbreak and areas of wind speed increase (negative reductions) were generally observed to the sides of the windbreaks. The greatest reductions were observed between about 3h and 6h downstream of the windbreak. On the sloping surfaces of the pile, reduction factors of 5 to 10% were observed upstream of the three windbreaks placed near the leading edge and negative reduction factors in the lee of the pile downstream of the windbreaks. A windbreak placed near the centerline caused wind speed reductions upstream, as well as downstream, of the windbreak on the pile top (Figure 6.13(a)). The area of coverage and magnitude of the

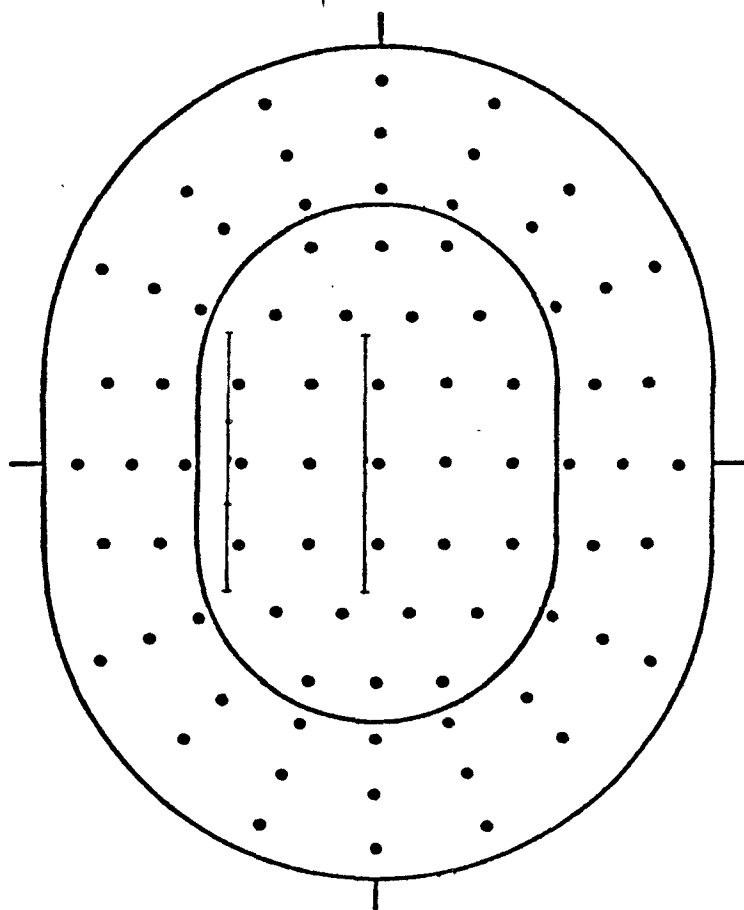


Figure 6.11 Sketch of windbreak positions with respect to thermistor positions on the top of the oval, flat-topped pile.

flow  
direction

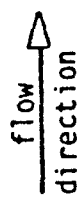
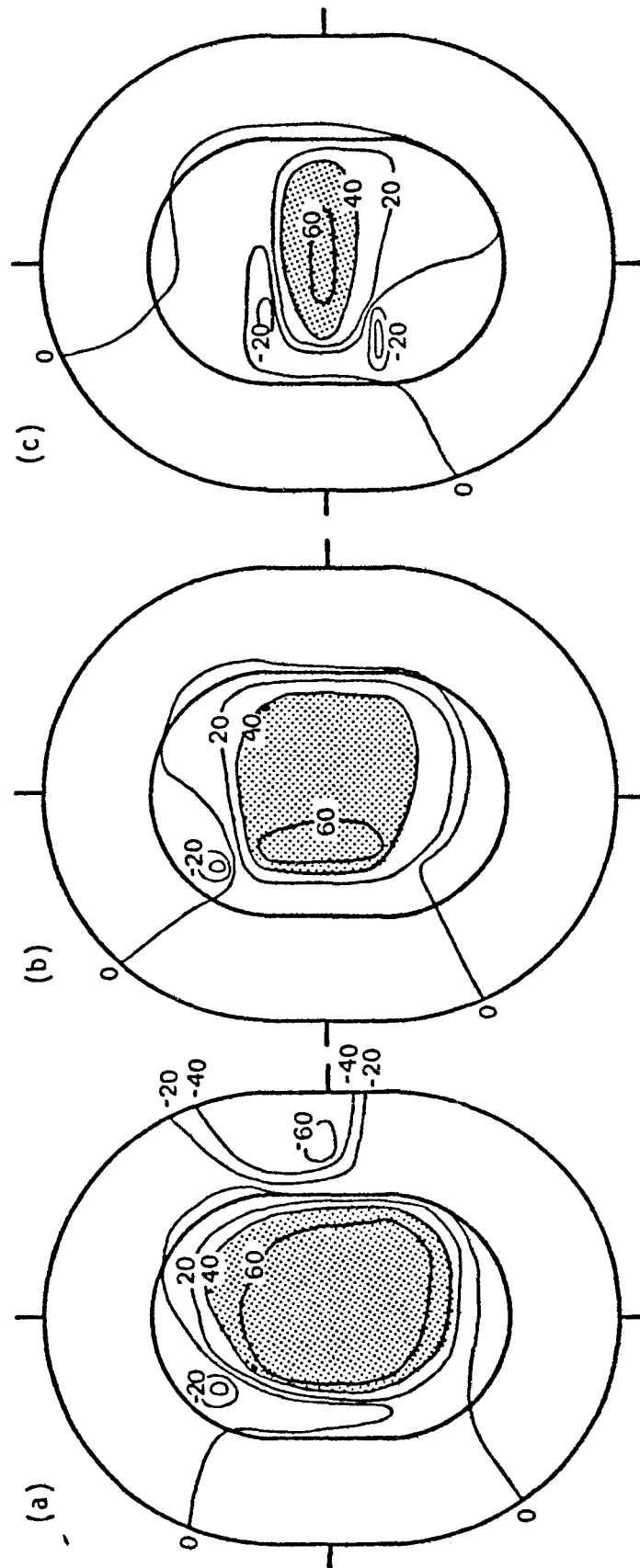



Figure 6.12 Wind speed reduction factor for the 65% porous windbreak placed near the pile leading edge: (a) height 0.27H and length 0.5T, (b) height 0.14H and length 0.5T, (c) height 0.27H and length 0.16T.

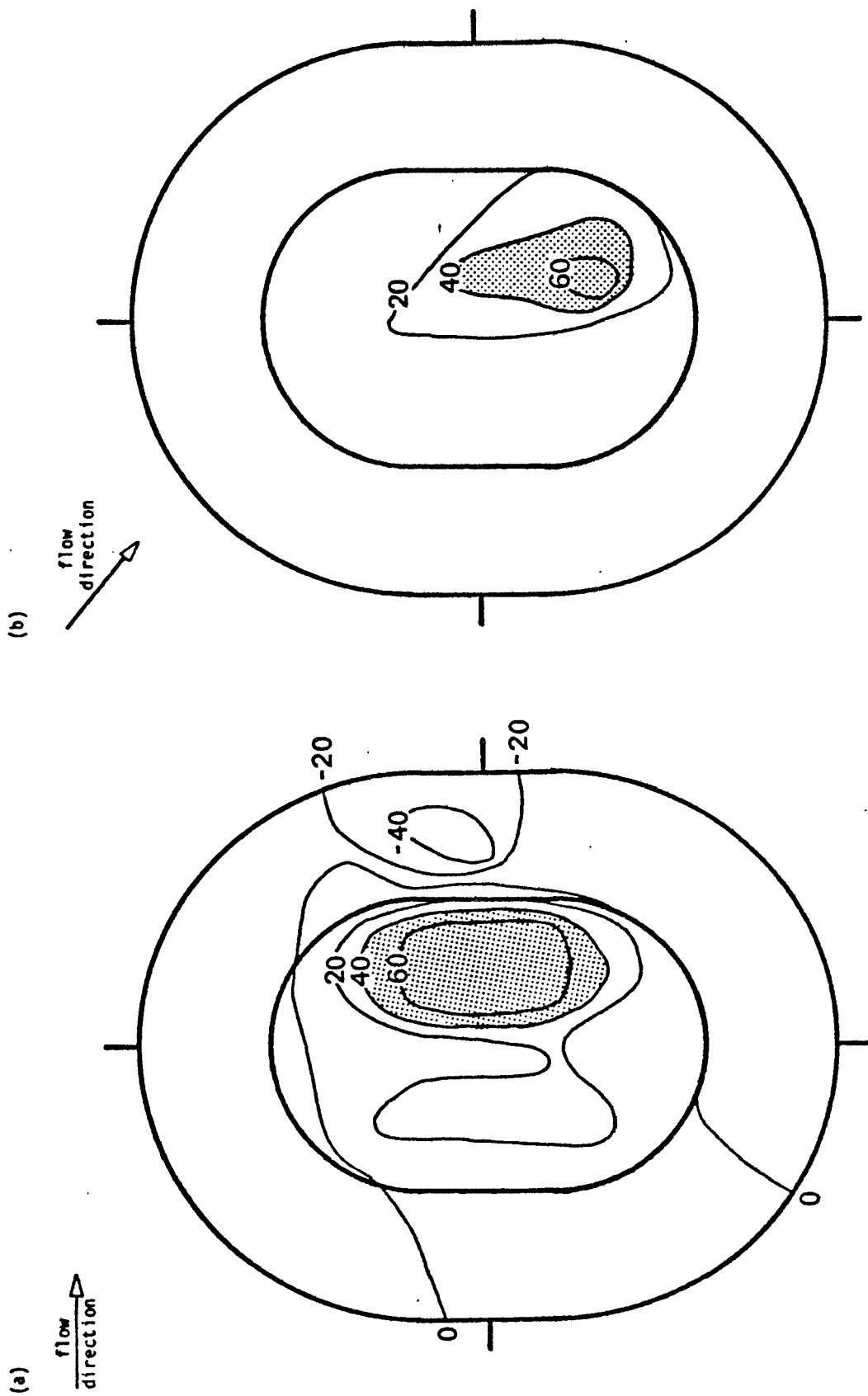


Figure 6.13 Wind speed reduction factor for the 65% porous windbreak of height  $0.27H$  and length  $0.5T$  placed near the pile centerline. Pile is: (a) normal, (b)  $40^\circ$  to incident flow.

reductions were greater for a higher windbreak. Reduction factors for the  $0.14H$  high,  $0.5T$  long windbreak placed near the centerline with the incident flow  $40^\circ$  to the windbreak normal clearly show that the area of coverage shifted with the wind direction (Figure 6.13(b)). Smaller reductions were observed on the slope downstream of the windbreak. Here the reduction factor was defined with respect to the no windbreak case with the pile at  $40^\circ$  to the flow.

To summarize, windbreaks on the pile top reduce wind speeds on the top both upstream and downstream of the windbreak. Greater reductions were observed a distance  $3h$  to  $6h$  downstream of the windbreak than immediately in its lee. Small reductions occurred along the slope upstream of the windbreaks placed near the leading edge, but, in general, the areas of high wind speed without any windbreak were not affected. Hence windbreaks located on the top of the pile may not provide much protection against high winds, but may be used to locally protect regions on the top of the pile.

## 7. FURTHER ANALYSES AND DISCUSSION OF RESULTS

In this section, windbreak efficiencies based upon the relationships between particle uptake and wind speed are presented. Then the results of both parts of the experiment (flows about a windbreak and windbreak-protected piles) are compared to results of previous studies.

### 7.1 RELATION TO PARTICLE UPTAKE

Relative windbreak effectiveness may be assessed by several methods. Wind speed reduction patterns and the normalized maximum wind speed have been described. Further analyses based on particle uptake at wind speeds exceeding a threshold value will be described. Results for windbreaks placed upwind of the pile will be discussed first.

If emissions had been measured directly, the windbreak efficiency  $E$  would have been defined as

$$E = 1 - (Q/Q_0) \quad (7.1)$$

where  $Q$  and  $Q_0$  are the storage-pile fugitive-dust emission rates with and without the windbreak, respectively. Since wind speeds have been measured here, assumed relationships between wind speed and emissions are used to calculate efficiencies. Depending on the reference wind speed, the wind speed on the lee side of the piles and on part of the top of the oval, flat-topped pile in the absence of any windbreak may be less than the threshold. In general, with certain windbreaks, the speeds in these regions could become greater than the threshold. Furthermore, a windbreak may reduce wind speeds to values less than the threshold over part or all of the pile. Hence a better definition of efficiency would include a threshold value. However, threshold speeds

have been determined only for a few cases as discussed in section 2.1. The relationship between threshold speed and particle size and moisture content is not understood. If a given threshold speed were applied to the data here, a full-scale reference wind speed would have to be assumed. To a first approximation, it is assumed here that the reference wind speed is sufficiently high that wind speeds everywhere, with and without a windbreak, exceed the threshold. Percentage efficiencies  $E_1$  and  $E_3$  are defined based upon linear and cubic relations between wind speed and particle uptake, respectively. Hence

$$E_1 = [1 - \sum_i (u_i A_i) / \sum_i (u_{0,i} A_i)] \times 100 \quad (7.2)$$

$$E_3 = [1 - \sum_i (u_i^3 A_i) / \sum_i (u_{0,i}^3 A_i)] \times 100 \quad (7.3)$$

where the summation is over the entire pile. In effect, these efficiencies are  $1 - (\overline{u^n} / \overline{u_0^n})$ , where  $n$  is either 1 or 3 and  $\overline{u^n}$  and  $\overline{u_0^n}$  are the area-averaged values over the pile surface with and without a windbreak, respectively. Later in this subsection, as an example, threshold and reference wind speeds are assumed and the areal extent of erosion is noted for the various windbreaks.

Previous analyses by the present author of the data for the conical pile utilized an overall or area-averaged reduction factor,  $\overline{R} = \overline{1 - u_i / u_{i,0}}$ , and a windbreak effectiveness factor,  $E = \overline{1 - u_i^3 / u_{0,i}^3}$ , (Billman, 1984). However, if the objective was to define a parameter which is the fractional amount by which fugitive emissions have been reduced, then  $E_1$  and  $E_3$  would be better parameters than  $\overline{R}$  and  $E$ . In the previous analyses, if the wind speed at some points in the no windbreak case were zero, then  $\overline{R}$  or  $E$  would be infinite. In addition, the regions

of low wind speed in the absence of the windbreak make relatively large contributions to R and E. This limitation has been removed by using the terms  $E_1$  and  $E_3$  in the present analysis.

$E_1$  for the windbreaks placed upstream of the conical and larger piles with normal incident flow are given in Tables 7.1 and 7.2, respectively. In general, a windbreak is more effective (higher  $E_1$ ) when placed upstream of the conical pile, as compared to a windbreak of the same relative size placed upstream of the larger, oval-shaped pile. Trends in  $E_1$  with changes in height, length, location and porosity of the windbreak are similar for both piles. In general, increasing windbreak height is desirable. Efficiencies range from 28-45% and 13-21% for 0.5H high windbreaks placed upstream of the conical and larger piles, respectively, and for higher windbreaks, 44-77% and 27-62%, again for the two piles. The 1.5H height was more effective than the 1.0H height with the oval, flat-topped pile, reflecting increased wind speed reductions on the pile top for the highest windbreak. For most cases with the conical pile, windbreaks of heights 1.0H and 1.5H were equally effective, within experimental scatter. Efficiencies were higher with the less porous windbreak material. Except for the windbreaks of height one half the pile height (0.5H), efficiency was lower when the windbreak was not as long as the pile base length. Length was not significant for the 0.5H high windbreaks because only the lower part of the pile sides were significantly affected with the longer windbreak, not the higher part, the location of high wind speeds in the absence of any windbreak (refer to Figure 5.3). However, with a higher windbreak, increased length

TABLE 7.1 EFFICIENCY ( $E_1$ ) FOR THE VARIOUS WINDBREAKS PLACED UPSTREAM OF THE CONICAL PILE

65% porous windbreak					50% porous windbreak			
position:	1H		3H		1H		3H	
length:	1.0D	1.5D	1.0D	1.5D	1.0D	1.5D	1.0D	1.5D
height								
0.5H	34	32	28	30	46	45	36	36
1.0H	48	45	53	52	66	67	65	71
1.5H	47	44	55	54	64	65	71	77

TABLE 7.2 EFFICIENCY ( $E_1$ ) FOR THE VARIOUS WINDBREAKS PLACED UPSTREAM OF THE OVAL, FLAT-TOPPED PILE

65% porous windbreak					50% porous windbreak				
position:	1H		3H		1H			3H	
length:	0.6B	1.0B	0.6B	1.0B	0.6B	1.0B	1.5B	0.6B	1.0B
height									
0.5 H	15	16	13	----	18	20	21	15	17
0.75H	----	----	----	----	----	41	----	----	34
1.0 H	27	34	28	37	34	53	51	31	49
1.25H	----	----	----	----	----	56	----	----	57
1.5 H	33	39	38	----	44	58	59	43	62

caused wind speed reductions in the high wind speed area on the sides. For both piles, the windbreak locations of 1H and 3H upwind of the pile were better for the windbreaks of height 0.5H and 1.5H, respectively.

Tables 7.3 and 7.4 list  $E_3$ , the efficiency based upon the  $u^3$  relation to dust uptake for the various windbreak cases for the conical and larger piles, respectively. Again, the efficiencies tend to be higher with the conical pile. Many of the same qualitative results as with  $E_1$  are apparent. The trends are clearly seen in a plot of efficiency ( $E_3$ ) vs. windbreak height as functions of windbreak length and porosity for both piles (Figure 7.1). Windbreaks of the lowest height were least effective; windbreaks higher than the pile were significantly more effective only with the oval, flat-topped pile. Windbreaks shorter than the pile base length were less effective than those at least as long as the pile. The less porous material was clearly more effective. These trends were observed for windbreaks at either the 1H or 3H position.

Although the highest efficiencies of 99% and 96% correspond to the 50% porous material of height 1.5H, length 1.5 times the base diameter of the conical pile and equal to the base length of the oval, flat-topped pile, respectively, located 3H from the base of the piles, the efficiencies of the more economical windbreak of the same porosity, height equal to the pile height and length equal to the pile base length are only slightly lower (97% and 89%, respectively). Clearly, the latter size would be preferable on the basis of cost effectiveness. Any location between 1H and 3H from the base of the pile could be chosen depending on the convenience.

TABLE 7.3 EFFICIENCY ( $E_3$ ) FOR THE VARIOUS WINDBREAKS PLACED UPSTREAM OF THE CONICAL PILE

position: length: height	65% porous windbreak				50% porous windbreak			
	1H		3H		1H		3H	
	1.0D	1.5D	1.0D	1.5D	1.0D	1.5D	1.0D	1.5D
0.5H	74	72	66	67	82	80	76	76
1.0H	88	85	91	90	97	97	97	98
1.5H	86	82	92	91	95	95	98	99

TABLE 7.4 EFFICIENCY ( $E_3$ ) FOR THE VARIOUS WINDBREAKS PLACED UPSTREAM OF THE OVAL, FLAT-TOPPED PILE

position: length: height	65% porous windbreak				50% porous windbreak			
	1H		3H		1H			3H
	0.6B	1.0B	0.6B	1.0B	0.6B	1.0B	1.5B	0.6B 1.0B
0.5 H	42	45	39	----	48	49	51	45 50
0.75H	----	----	----	----	----	84	----	---- 74
1.0 H	63	74	66	79	73	92	89	70 89
1.25H	----	----	----	----	----	91	----	---- 95
1.5 H	67	73	75	----	80	92	92	81 96

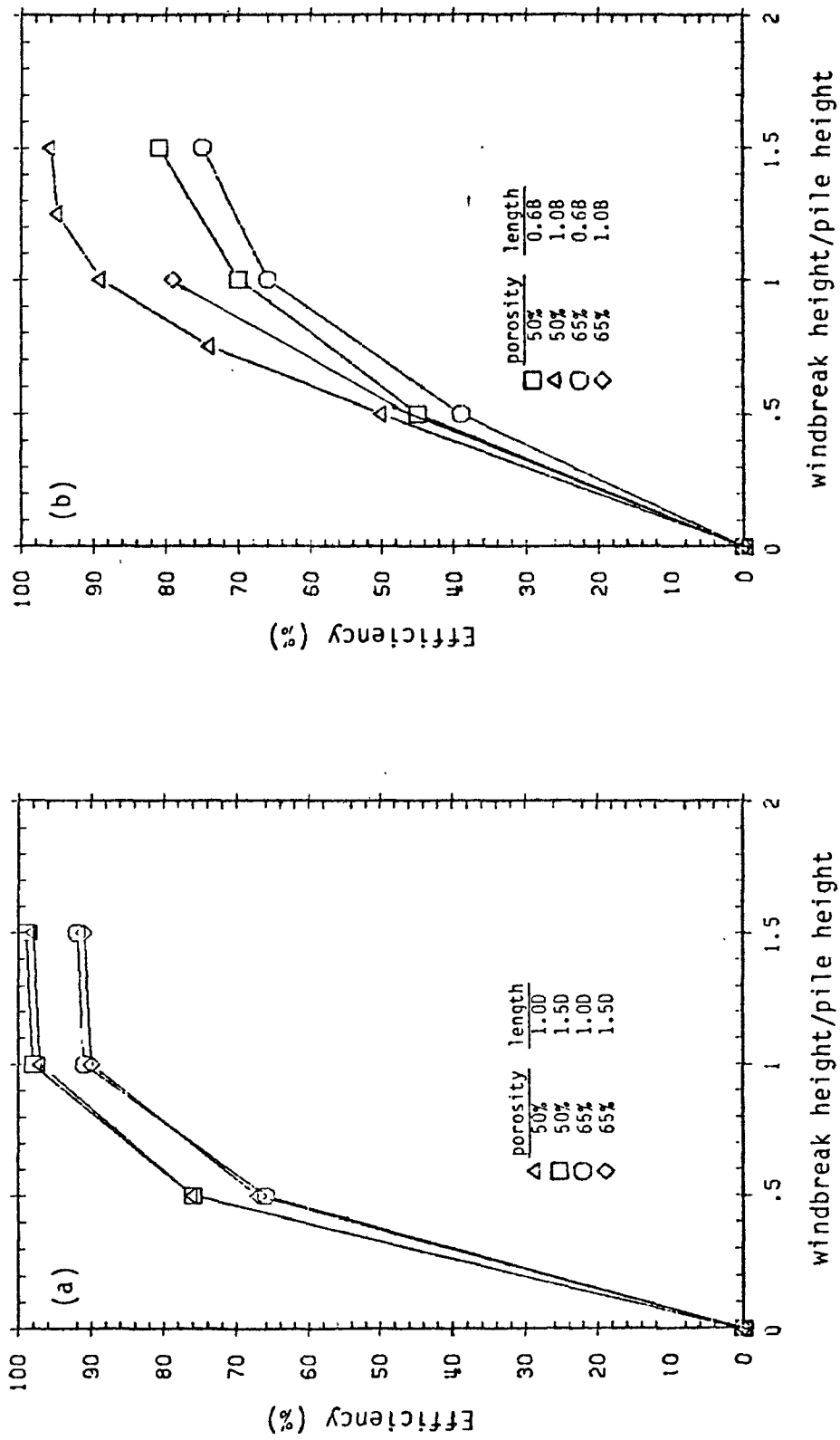


Figure 7.1 Efficiency ( $E_3$ ) vs. height for windbreaks placed 3H from the pile base: (a) conical pile, (b) oval, flat-topped pile.

As discussed earlier in this section, windbreak effectiveness may also be assessed by assuming threshold ( $u_t$ ) and full-scale reference ( $u_r$ ) speeds. An example calculation was made using the  $u/u_r$  wind tunnel data for windbreaks placed upwind, assuming a reference wind speed of 10 m/s and a threshold velocity of 2.8 m/s to determine the percentage surface area over which no emissions would occur (i.e. where  $u < u_t$ ). (This threshold speed was also used in an example calculation by Martin and Drehmel (1980), and may be applicable to some fine material). With no windbreak, 22% (25%) of the conical (oval) pile surface area had wind speeds less than the threshold. With all the 65% porous windbreaks and the 0.5H high 50% porous windbreaks, 40-65% (24-49%) of the pile surface area would have no dust emissions. The area increased to 77-100% (40-99%) for the other 50% porous windbreaks. Note that the percentage surface areas calculated here would increase with a decrease in reference speed and/or increase in threshold velocity.

For windbreaks placed on top of the larger pile, efficiencies ( $E_1$  and  $E_3$ ) were quite low, less than 12%. As discussed in section 6.2, wind speeds on the pile top were reduced significantly, but the windbreaks had very little effect in the high wind speed region on the windward face. This suggests that fugitive-dust emissions on the top of the pile may be controlled locally through the use of a windbreak. Since the windbreaks were not very high, (0.14H and 0.27H), in practice, they could be portable, providing protection to specific areas on the top of the pile, depending upon the location of activity and wind direction.

## 7.2 COMPARISON TO PREVIOUS STUDIES

Many results compare well with previous studies discussed in section 2, but several windbreak design guidelines are introduced here. The flow structure about a porous windbreak will be discussed first, then that about windbreak-protected piles.

The flow structure downwind of a porous windbreak was qualitatively similar to that observed by Raine and Stevenson (1977). The area of minimum wind speed and high turbulence intensity occurred not immediately, but farther downwind of the windbreak and turbulence was generated in the shear layer at the top of the windbreak. As observed by Perera (1981), the hot-wire anemometer (HWA) overpredicted wind speeds in the highly turbulent region. Also, for heights greater than the windbreak height, the longitudinal turbulence intensity, measured with the pulsed-wire anemometer (PWA), was greater than that measured with the HWA. However, unlike that observed by Perera, the intensity was less when measured with the PWA for heights less than  $1h$  and the mean wind speed measured by the two instruments was approximately the same for heights above about  $2h$ . Perera used a solid barrier (0% porous); here it was 50% porous.

Results with the windbreak-protected piles may be compared with two previous laboratory studies in which windbreaks were located upwind of a pile. Davies (1980) recommended a windbreak height of  $1.4H$ , which, based on our results, should be very good. We did not examine the case of a windbreak of varying porosity as Davies did. However, our results cannot adequately be compared with those by Davies since only the final result was reported, not the details of the various cases tested. The

present work extends that reported by Soo et al. (1981) and Cai et al. (1983). In both studies, optimal windbreak location was found to be related to the windbreak height, and lower wind speeds were observed with less porous windbreaks. In the present study, with three-dimensional piles, effects of windbreak length, additional windbreak heights and porosities, and various incident flow directions were examined.

Windbreak efficiencies presented here are generally much higher than those estimated by Bohn et al. (1978) and Jutze et al. (1977), indicating that windbreaks may be a highly effective fugitive-dust control method.

## 8. CONCLUSIONS

This wind tunnel study has shown that windbreaks normal to the wind direction placed upwind of a conical and a larger, oval, flat-topped storage pile reduce wind speeds near the surface of the pile and hence suggest reductions in fugitive-dust emissions. Of the windbreaks tested for each pile, the largest (height 1.5 times the pile height (1.5H) and length equal to the larger pile base length (1.0B) or 1.5 times the conical pile base diameter (1.5D)) 50% porous windbreak placed 3H from the pile appears to be best in terms of greatest wind speed reduction. However, all the 50% porous windbreaks at least as high as the pile and as long as the pile base had similar overall effects. Windbreaks of height and/or length less than that of the pile were clearly less effective. Optimal windbreak location appears to be related to windbreak height, particularly for the conical pile; the higher the windbreak, the farther it should be located upwind of the pile. However, locations farther than 3H were not examined. A farther location could be more effective, but the pile could then be beyond the sheltered region, hence, a less effective windbreak position. Windbreaks of height 1.5H caused greater wind speed reductions on the top of the oval, flat-topped pile than those of height equal to or less than the pile height, but the difference in the effectiveness of 1.0H and 1.5H high windbreaks with the conical pile was not significant.

Windbreak length and position are even more important in determining effectiveness when the air flow is not normal to a windbreak. With a windbreak of height and length equal to the pile dimensions, fairly high wind speed reductions resulted when the

windbreak was placed upwind normal to the flow and also at an angle of  $20^\circ$  to the normal, but very little reduction occurred at an angle of  $40^\circ$ .

Windbreaks ( $0.14H$  and  $0.27H$  high) placed on the top of the oval, flat-topped pile caused large areas of high wind speed reductions on the pile top both downwind and upwind of the windbreak, but very small reductions to the high wind speeds on the windward face occurring in the absence of any windbreak. The area of greatest reduction was not immediately downwind of the windbreak, but displaced farther downstream. Changes in wind direction shifted the location of the sheltered region. These results suggest that fugitive-dust emissions may be locally controlled with windbreaks placed on the top of a relatively level storage pile. In particular, portable windbreaks may be quite practical since they could be positioned to protect active areas of the pile.

Design guidelines developed by Soo et al. (1981) and Cai et al. (1983) have been extended since more windbreak configurations were examined and three-dimensional piles were used. Windbreak efficiencies were generally much higher than expected (Bohn et al., 1978 and Jutze et al., 1977). With the design guidelines presented here, the use of windbreaks for fugitive-dust control appears promising.

Wind speed was isolated here as the major factor affecting storage-pile fugitive-dust emissions, but storage-pile moisture content, type of material stored and threshold speed also affect emissions. A clearer understanding of the relationship of wind speed and threshold speed to fugitive-dust emissions would allow for better analysis of the data presented. Additional field measurements of fugitive dust from storage

piles with and without windbreaks would be helpful for comparison to the efficiencies and design guidelines presented here.

## 9. REFERENCES

- Axetell, Jr., K., 1978: Survey of fugitive dust from coal mines. EPA-908/1-78-003, EPA Region VIII, Office of Energy Activities, Denver, CO 80295.
- Bagnold, R.A., 1941: The Physics of Blown Sand and Desert Dunes. Methuen, London, 265 pp.
- Billman, B.J., 1984: Windbreak effectiveness for the control of fugitive-dust emissions from storage piles -- A wind tunnel study. Presented at the Fifth Symposium on the Transfer and Utilization of Particulate Control Technology, Kansas City, MO, August 27-30, 1984. Proceedings to be published by the Environmental Protection Agency and Electric Power Research Institute.
- Blackwood, T.R. and Wachter, R.A., 1978: Source assessment: Coal storage piles. EPA-600/2-78-004k, U.S. Environmental Protection Agency, Cincinnati, OH.
- Bohn, R., T. Cuscino, and C. Cowherd, Jr., 1978: Fugitive emissions from integrated iron and steel plants. EPA-600/2-78-050. U.S. Environmental Protection Agency.
- Bradbury, L.J.S. and I.P. Castro, 1971: A pulsed-wire technique for velocity measurements in highly turbulent flows. *J. Fluid Mech.* 49: 657.
- The Bureau of National Affairs, Inc., 1983: Environment Reporter. 336:0553-0554, Rule 302(f).
- The Bureau of National Affairs, Inc., 1982: Environment Reporter. 411:0516-0517, R336.1371, R336.1372.
- Caborn, J.M., 1957: Shelterbelts and microclimate. *Forestry Commun. Bull.* 29:1.
- Cai, S., Chen, F.F., and Soo, S.L., 1983: Wind penetration into a porous storage pile and use of barriers. *Environ. Sci. Technol.* 17: 298.
- Caput, C., Belot, Y., Guyot, G., Samie, C., and Seguin, B., 1973: Transport of a diffusing material over a thin wind-break. *Atmos. Environ.* 7: 75.
- Castro, I.P., and W.H. Snyder, 1982: A wind tunnel study of dispersion from sources downwind of three-dimensional hills. *Atmos. Environ.* 16: 1869.
- Counihan, J., 1975: Adiabatic atmospheric boundary layers: A review and analysis of data from the period 1880-1972. *Atmos. Environ.* 9: 871.

- Cowherd, Jr., C., K. Axetell, Jr., C.M. Guenther, and G. Jutze, 1974: Development of emission factors for fugitive dust sources. EPA-450/3-74-037, U.S. Environmental Protection Agency, Office of Air Quality Planning and Standards.
- Cowherd, Jr., C., R. Bohn, and T.A. Cuscino, 1979: Iron and Steel plant open source fugitive emission evaluation. EPA-600/2-79-103. U.S. Environmental Protection Agency, Research Triangle Park, NC.
- Cowherd, Jr., C., 1982: Emission factors for wind erosion of exposed aggregates at surface mines. Proc. 75th APCA Annual Meeting. Paper 82-15.5.
- Currier, E.L. and B.D. Neal, 1984: Fugitive emissions from coal-fired power plants. EPRI CS-3455. Electric Power Research Institute, Palo Alto, CA.
- Cuscino, T., G.E. Muleski, and C. Cowherd, Jr., 1983: Iron and steel plant open source fugitive emission control evaluation. EPA-600/2-83-110. U.S. Environmental Protection Agency, Office of Research and Development, Research Triangle Park, NC.
- Davies, A.E., 1980: A physical modelling approach to the solution of fugitive emission problems. Proc. 73rd APCA Annual Meeting. Paper 80-68.11.
- U.S. Environmental Protection Agency, 1983: Supplement No. 14 for Compilation of Air Pollutant Emission Factors, 3rd ed., AP-42, Research Triangle Park, North Carolina.
- Gandemer, J. 1981: The aerodynamic characteristics of windbreaks, resulting in empirical design rules. J. of Wind Engineering and Industrial Aerodynamics. 7: 15.
- Gillette, D., 1978a: A wind tunnel simulation of the erosion of soil: Effect of soil texture, sandblasting, wind speed, and soil consolidation on dust production. Atmos. Environ. 12: 1735.
- Gillette, D., 1978b: Tests with a portable wind tunnel for determining wind erosion threshold velocities. Atmos. Environ. 12: 2309.
- Gillette, D.A., J. Adams, A. Endo, and D. Smith, 1980: Threshold velocities for input of soil particles into the air by desert soils. J. Geophys. Res. 85(C10): 5621, October 20, 1980.
- Jacobs, A., 1984: The flow around a thin closed fence. Boundary-Layer Meteorology. 28: 317.
- Jensen, M., 1958: The model-law for phenomena in a natural wind. Ingenioren, Int. Ed. Vol. 2, No. 4.

- Jutze, G.A., J.M. Zoller, T.A. Janszen, R.S. Amick, C.E. Zimmer and R.W. Gerstle, 1977: Technical guidance for control of industrial process fugitive particulate emissions. EPA-450/3-77-010, U.S. Environmental Protection Agency, Office of Air Quality Planning and Standards.
- Lawson, Jr., R.E. and R.E. Britter, 1983: A note on the measurement of transverse velocity fluctuations with heated cylindrical sensors at small mean velocities. *J. Physics E: Sci. Instrum.* 16: 563.
- Martin, D.J. and D. Drechsel, 1980: Control methods for fugitive area sources. *Proc. Fourth Symposium on Fugitive Emissions, Measurement and Control*. EPA-600/9-80-041, U.S. Environmental Protection Agency, Office of Research and Development, Research Triangle Park, NC, p. 402
- Mulhearn, P.J. and E.F. Bradley, 1977: Secondary flows in the lee of porous shelterbelts. *Boundary Layer Meteorol.* 12: 75.
- Naegeli, W., 1953: The braking effect of a forest on wind. *Internat. Union Forestry Res. and Organisation*, 11th Congr. Rome. Section 11, pp. 12-17. In: *Windbreaks and Shelterbelts*. WMO Technical Note No. 59. Van Eimern, et al., eds.
- Ogawa, Y. and P.G. Diosey, 1980: Surface roughness and thermal stratification effects on the flow behind a two-dimensional fence. II. A wind tunnel study and similarity considerations. *Atmos. Environ.* 14: 1309.
- Pendergrass, W., and S.P.S. Arya, 1984: Dispersion in neutral boundary layer over a step change in surface roughness--I. Mean flow and turbulence structure. *Atmos. Environ.* 18: 1267.
- Perera, M.D.A.E.S., 1981: Shelter behind two-dimensional solid and porous fences. *J. Industrial Aerodynamics.* 8: 93.
- Raine, J.K. and Stevenson, D.C., 1977: Wind protection by model fences in a simulated atmospheric boundary layer. *J. Industrial Aerodynamics.* 2: 159.
- Rasmussen, R.A., 1962: Application of thermistors to measurements in moving fluids. *Rev. Sci. Instrum.* 33: 38.
- Seginer, I., 1975a: Atmospheric stability effect on windbreak shelter and drag. *Boundary Layer Meteorol.* 8: 383.
- Seginer, I., 1975b: Flow around a windbreak in oblique wind. *Boundary Layer Meteorol.* 9: 133.

- Snyder, W.H., 1979: The EPA meteorological wind tunnel--It's design, construction and operating characteristics. EPA-600/4-79-051. U.S. Environmental Protection Agency, Office of Research and Development Research Triangle Park, NC.
- Snyder, W.H., 1981: Guideline for fluid modeling of atmospheric diffusion. EPA-600/8-81-009, U.S. Environmental Protection Agency, Research Triangle Park, NC.
- Soo, S.L., J.C. Perez, and S. Rezakhany, 1981: Wind velocity distribution over storage piles and use of barriers. Proc. Symposium on Iron and Steel Pollution Abatement Technology for 1980. EPA-600/9-81-017, U.S. Environmental Protection Agency, Office of Research and Development, Research Triangle Park, NC.
- Thorntwaite, C.W., 1931: The climates of North America according to a new classification. The Geographical Review. 21: 633.
- Townsend, A.A., 1956: The Structure of Turbulent Shear Flow. Cambridge University Press, Cambridge, England, 315 pp.
- Van Eimern, J., Karschon, R., Razumova, L.A., and Robertson, G.W., 1964: Windbreaks and shelterbelts. WMO Technical Note No. 59. 188 pp.